A new modal analysis method to put constraints on the aqueous alteration of CR chondrites and estimate the unaltered CR composition

M. PERRONNET [1*], M. E. ZOLENSKY [1], M. GOUNELLE [2], C. S. SCHWANDT [1]

[1] Lyndon B. Johnson Space Center, KT, 2101 Nasa Road One, Building 31, Houston, TX 77058-3696, USA

[2] Laboratoire d'Etude de la Matière Extraterrestre, Museum National d'Histoire Naturelle, CP52, 57 rue Cuvier, 75231 Paris cedex 05, France

*Corresponding author. E-mail: murielle.c.perronnet@nasa.gov

ABSTRACT

CR carbonaceous chondrites are of the major interest since they contain one of the most primitive organic matters. However, aqueous alteration has more or less overprinted their original features in a way that needed to be assessed. That was done in the present study by comparing the mineralogy of the most altered CR1 chondrite, GRO 95577, to a less altered CR2, Renazzo. Their modal analyses were achieved thanks to a new method, based on X-ray elemental maps acquired on electron microprobe, and on IDL image treatment.

It allowed the collection of new data on the composition of Renazzo and confirmed the classification of GRO 95577 as a CR1. New alteration products for CRs, vermiculite and clinochlore, were observed. The homogeneity of the Fe-poor clays in the CR1 and the distinctive matrix composition in the two chondrites suggest a wide-range of aqueous alteration on CRs. The preservation of the outlines of the chondrules in GRO 95577 and the elemental transfers of Al, Fe and Ca throughout the chondrule and of Fe and S from the matrix to the chondrule favor the idea of an asteroidal location of the aqueous alteration.

From their mineralogical descriptions and modal abundances, the element repartitions in Renazzo and GRO 95577 were computed. It indicates a possible relationship between these two chondrites via an isochemical alteration process. Knowing the chemical reactions that occurred during the alteration, it was thus possible to decipher the mineralogical modal abundances in the unaltered CR body.

INTRODUCTION

The CR carbonaceous chondrites (CRs), based on their enrichments in the heavy isotopes of nitrogen and hydrogen (Kung and Clayton 1978; Kolodny et al. 1980; Bischoff et al. 1993a; Weisberg et al. 1993; Alexander et al. 1998) and their unique petrology (McSween 1977; Kolodny et al. 1980; Frederiksson et al. 1981; Kallemeyn and Wasson 1982; Bischoff et al. 1993 a; Bischoff et al. 1993b) and their primitive organic matter (e.g. Pearson et al. 2006) are proposed to be among the most primitive extraterrestrial materials available for study (e.g. Ash et al. 1993; Pearson et al. 2006; Abreu and Brearley 2006).
But, aqueous alteration has more or less overprinted their original features (Zolensky et al. 1989; Zolensky 1991; Weisberg et al. 1995). The problem is that even if the general characteristics of alteration in CRs are known (e.g., Weisberg et al. 1993; Zolensky et al. 1993; Noguchi 1995), the details of alteration (the elementary physico-chemical reactions as well as the nebular and/or asteroidal location) are lacking in comparison with CM or CI chondrites (Brearley 2006) and are still in debate.
The petrologic type, from 3 to 1, is an indicator of the increasing degree of aqueous alteration. Zolensky and Browning (1994) reported that CM chondrites exhibit the complete petrologic range from 2 to 1. On the contrary, most of the CRs are of petrologic type 2 (more than 2 dozens of unpaired samples) and no clear evidence for CR3 exists at this time. Smith et al. (2004) reported two samples as being potential CR3 chondrites, NWA 1152 and SAH 00182, but a discussion is still going on because these samples have affinities both with CRs and CVs. At the opposite, the Grosvenor Mountains 95577 chondrite (GRO 95577), which has been first reported as a C2 chondrite (Mason 1997), was reevaluated as the first known CR1 by Weisberg and Prinz (2000). Do CR chondrites exhibit a complete petrologic range from 2 to 1 like CMs? To answer to this question the mineralogies of Renazzo, which is a mildly altered fall and one of the most typical CR2s, and of GRO 95577 were characterized by quantifying the proportion of each mineral phase. A new modal analysis method based on X-ray elemental maps acquisition on electron microprobe was used for this purpose (Schwandt et al. 2001; Schwandt and McKay 2005; Schwandt 2006a,b). This study results in the estimation of what would be the unaltered CR body. Finally, new arguments concerning the mechanisms of the aqueous alteration process and its location are exposed.

SAMPLES AND TECHNIQUES

One thick section of Renazzo (partly represented on Figure 1) (Renazzo-719) was lent by the Museum National d'Histoire Naturelle in Paris and two thick sections of GRO 95577 (Figure 2) were prepared at NASA-JSC from the chips lent by the Meteorite Working Group.

Images and compositions of silicate minerals as well as opaque phases were obtained by using a JEOL JSM-5910LV Secondary Electron Microscope (SEM used at 15 keV) and a Cameca SX-100 electron microprobe (EMP) in WDS mode using appropriate silicate and metal standards. Operating conditions for the EMP were 15 keV accelerating voltage with a 20 nA beam current for silicates and 20 keV accelerating voltage with a 40 nA beam current for metals. The diameter of the electron beam was 1 μm.

Modal abundances of the mineral and metallic phases in Renazzo and GRO 95577 were assessed using a new method developed by Schwandt (Schwandt et al. 2001; Schwandt and McKay 2005; Schwandt 2006a,b). It consists of first acquiring the X-ray elemental maps for Fe, Ni, S, Si, Al, Mg and Ca on the EMP. The accelerating voltage is 20 keV with a 40 nA

beam current. The spot diameter is 1 μm and the dwelltime is 5 to 30 ms. With a resolution of 1 or 2 μm per pixel, we are able to map areas whose size ranges up to 3600*3600 pixel^2 in about 72 hours. Then, for each elemental map, using the IDL software, the intensity of the signal is known in each pixel. To illustrate the use of this method, we are describing it for Renazzo.

Schwandt (Schwandt et al. 2001; Schwandt and McKay 2005; Schwandt 2006a,b) found that it is convenient to identify silicates on the map of the ratio (Mg+Ca+Fe)/(Si+Al). This one represents the ratio of cations usually octahedrally coordinated over cations usually tetrahedrally coordinated in the mineral structures. For each pixel, this ratio, which is called octovertet, is computed by the IDL software and is mapped on Figure 1a. The color of the pixel changes from purple – blue – green – yellow – orange to red as the intensity of this ratio increases. Knowing the mineralogy of Renazzo thanks to the SEM and EMP analyses, it is possible to discriminate some phases according to the intensity of the octovertet signal. On Figure 1a there are the group I with kamacite (1), low-Ni kamacite (2), intermediate sulfide phases (3) and Ca-carbonate (11) in red, the group II with Fe-rich olivine matrix (4) in light green, the group III with the feldspathic mesostasis in dark blue, the group IV with chamosite mesostasis (6), olivine (7), Fe-olivine (8) in bright green and the group V with enstatite (9) and augite (10) in light blue. But it appears that using the Fe map, we can distinguish kamacite (1), low-Ni kamacite (2) in red from intermediate sulfide phases (3) in green, which are a family of phases intermediate between pyrrhotite and pentlandite (Scott and Taylor 1985; Alexander et al. 1989; Zolensky and Thomas 1995; Chokai et al. 2004). To distinguish, kamacite (1) and low-Ni kamacite (2), we are using the Ni map on which they are respectively in red and green. Then to distinguish chamosite ($(Si_3Al)(Fe^{2+},Mg,Fe^{3+})_5O_{10}(OH)_8$) mesostasis (6) from olivine (7) and Fe-olivine (8), we are using the Fe signal on which they are respectively in blue, purple and light blue. Finally on the Ca map, enstatite (9) in purple can be distinguished from augite (10) in orange. This map is also used to quantify Ca-carbonate (11). Then each mineral and metallic phase is defined by the range of its octovertet, Fe, Ni, Ca, S signals, so that the IDL software is able to quantify the number of pixels occupied by each phase. Thus, we can get the area% of each phase. The conversion from area% to vol% is discussed later.

RESULTS

Renazzo

The mineralogical studies of Renazzo have been made by Mason and Wiik (1962), Wood (1967), Nelen et al. (1975), McSween and Richardson (1977), Zolensky et al. (1991), Zolensky et al. (1993) and Weisberg et al. (1993). These authors indicate the composition of olivine, pyroxene and mesostasis in the chondrule as well as the matrix composition. The FeNi metal was studied by, e.g., Zanda et al. (1991), Lee et al. (1992), Weisberg et al. (1993) and Connolly et al. (2001) but information on sulfide phases is scarce (Zolensky 1991; Weisberg et al. 1993). This is one of the reasons we present a new description of Renazzo. Table 1 to Table 6 present the new modal data and mineral compositions which are compared to data in the literature.

Chondrules. Chondrules are mostly type I (Figure 1b) and consist in olivine and pyroxene (Porphyritic Olivine Pyroxene (POP) and Porphyritic Pyroxene (PP)) embedded in a feldspathic mesostasis. On Ren-719 thick section, one type II chondrule (Figure 1c) is observed having Fe-olivine (Fo_{66}) and a chamosite mesostasis (Figure 1d, Table 1 and Table 2). In type I chondrules, olivine grains are Fo_{99} in composition and most of the pyroxenes are enstatite (Fs_4Wo_1) which coexist minor few augite and pigeonite (Figure 3 and Table 1). The

feldspathic mesostasis is An_{96} in composition (Table 2). The main part of the metallic phases (Table 3) consists of blebs of low-Ni kamacite ($Fe_{0.95}Ni_{0.05}$), which are rimming the chondrules (Figure 1b). Typically few kamacites ($Fe_{0.90}Ni_{0.1}$) are observed as blebs inside the chondrule. Intermediate sulfide phases, whose composition is intermediate between pyrrhotite and pentlandite (Chokai et al. 2004), are observed at the periphery of the type II chondrule (Figure 1c). Sparse Ca-carbonate grains are only observed at the boundary between chondrule and matrix (Figure 1b).

Matrix. Matrix is fine-grained (Figure 1e) and Fe-olivine is the dominant mineral (Zolensky et al. 1991) (Table 4). Bibliographic data indicate that there is 0.7 vol% of S in Renazzo (Weisberg et al. 1993), which is mostly within the matrix (Zolensky 1991). That is confirmed by the X-ray map of S (see following paragraph). It is likely that these fine-grained sulfides are pyrrhotite, considering the low degree of aqueous alteration.

Modal abundance analysis. X-ray maps of Ca, Fe, Ni, S as well as octovertet, the ratio of (Fe+Mg+Ca) over (Si+Al), are shown on Figure 1a. These maps are oriented as the reflexion in a mirror of area e from Figure 1. As for a reminder, on the X-ray elemental map color changes from purple to red with respect to the intensity of the signal. On Figure 1a, the number associated to octovertet and to the element name corresponds to the maximal intensity of the signal. So, Fe (Fe 190) has the widest range in intensity and S (S 10) the lowest one.

As mentioned in the Sample and Techniques section, because of the crystal chemical selectivity of the octovertet map, we can distinguish metal and Ca-carbonate (red), chamosite mesostasis - olivine- Fe-olivine (bright green), matrix (light green), pyroxene (light blue) and feldspathic mesostasis (dark blue). The comparison between Fe and Ca maps allows one to distinguish metal and Ca-carbonate. Moreover, by looking at octovertet and Ca maps, enstatite (purple on Ca map) can be discriminated from the few augites (orange on Ca map). Fe, S and Ni maps show that the matrix has a homogeneous composition in these three elements but is richer in Fe and S than in Ni. The comparison of Ni and Fe maps reveals that kamacite (red on Ni map), is mainly inside the chondrule, whereas low-Ni kamacite (green on Ni map) is mainly at the periphery of the chondrule. On Fe map, the type II chondrule is easily distinguished from type I chondrules because its Fe signal is more intense (blue is lighter). The presence of intermediate S phases at the periphery of this type II chondrule is revealed by high intensity on Fe (green), Ni (red) and S (red) maps.

Each mineral and metallic phase is uniquely described by its range in intensity on octovertet, Fe, Ni, Ca, S signals. This information is input data for the IDL software in order to compute the number of pixels occupied by each phase. The modal analysis of a 109 mm^2 area (Figure 1a) indicates that in chondrules, pyroxenes account for 23 area% (20.7 area% of enstatite, 1.15 area% of augite and 1.15 area% of pigeonite), olivine for 19.2 area% (18.2 area% of Fo_{99} and 1 area% of Fo_{66}). The mesostasis is composed by feldspar (2.8 area%) and by chamosite (1.4 area%). A good description of opaque phases is possible thanks to this technique: they are low-Ni kamacite 3.3 area%, kamacite 0.7 area% and intermediate sulfide phases 0.9 area%. Ca-carbonates accounts for 0.8 area%, while the Fe-olivine rich matrix is the most important fraction with 47.9 area%. The comparison with the available data from literature is presented in the discussion part along with a debate on how to convert the area% in vol%.

GRO 95577

As noted in the introduction, the study of GRO 95577 was initiated by Weisberg and Prinz (2000). They noted that a remarkable replacement process, which preserved the texture of the initial chondrite, changes olivine and pyroxene into serpentine within chondrule, feldspar into

Al-chlorite within the mesostasis and kamacite blebs into magnetite. It is a near perfect pseudomorphic process. The authors reported also that the matrix represents more than 30 vol% and consists of phyllosilicates, magnetite, sulfides and carbonates. But, to constrain the physico-chemical conditions under which the aqueous alteration occurred, we have first to perform a more detailed description of the mineralogy of GRO 95577 along with its modal analysis.

Chondrules. The outlines of chondrules (Figure 2) are still visible but they now consist almost entirely of phyllosilicates (Figure 2a, b and c) having a particular composition, which is reported in Table 6. From this composition, structural formula are established considering a TO (kaolin-serpentine), a TOT (pyrophyllite-talc, smectite, vermiculite, mica) and a TOT O' (chlorite) structure. The structural formula is only reasonable for a TOT structure with Fe in its fully oxidized form. These phyllosilicates are $(Si_{2.84}Fe^{3+}_{0.90}Al_{0.22}Cr^{3+}_{0.05})(Mg_{2.73}Fe^{3+}_{0.27})Na_{0.15}Mg_{0.35}$ per $O_{10}(OH)_2$. Relative to tetrahedrally coordinated cations, the substitution is much too important for assuming that this mineral is a saponite, but with respect to Caillere et al. (1982), such a formula is typical of trioctahedral vermiculite, in which Fe^{3+} for Mg substitutions are reported in both the tetrahedral and octahedral sites. The Al-rich chlorite mesostasis, reported by Weisberg and Prinz (2000), was not observed in our thick sections but we do observe a MgAlFe chlorite mesostasis (Figure 2b and c). Two families are defined with respect to their Fe content (Clin. 1 and Clin 2. in Table 2). With respect to Bayliss (1975) nomenclature for trioctahedral chlorites, these are clinochlore. Their compositions are compared to the ones of phyllosilicates from the chondrules of CRs, CMs and CV chondrites in a Mg-Fe-Si+Al ternary diagram (Figure 4), which will be discussed later. Their structural formulae per $O_8(OH)_{10}$ are:

- $(Si_{3.28}Al_{0.72})(Al_{0.97}Mg_{2.03})(Al_{0.07}Mg_{0.96}Fe^{2+}_{1.71}Ca_{0.06}Mn_{0.04}\square_{0.16})$ for Clin. 1 ;
- $(Si_{3.23}Al_{0.77})(Al_{0.99}Mg_{2.01})(Al_{0.13}Mg_{0.74}Fe^{2+}_{1.90}Ca_{0.01}Mn_{0.05}\square_{0.17})$ for Clin. 2 .

Concerning the opaque phases (Table 3), we do not observe any large magnetite-rich chondrules but we do observe relics (67 μm mean) of kamacite. The blebs are quite often low-Ni in composition (3.4 wt% Ni) (Figure 2d) and one bleb exhibits zoning (Figure 5), with the inner part being richer in Ni (12.7 wt% Ni). This inner part of the bleb is probably a remnant of the initial kamacite. Pyrrhotite (Figure 2e) and pentlandite are observed but the intermediate S phases are the predominant S-bearing phases (Figure 2f). Within chondrules, huge Ca-rich carbonates grains are observed (533-640 μm in size). They enclose pentlandite, pyrrhotite and vermiculite (Figure 2a). Rims around chondrules are well defined and consist of serpentine having the same composition as the matrix (Table 4). Grains of framboidal magnetite, bleb of kamacite, pyrrhotite and intermediate sulfides are also found within the rims (Figure 2a).

Matrix. The composition of the fine-grained (Figure 2g) matrix is reported in Table 4. Sulfides (no bigger than 5 μm) and magnetite are visible. Huge Ca-rich carbonates grains are also found within the matrix (Figure 2h).

Whether previously resident in chondrules or in matrix, anhydrous minerals are no longer observed.

Modal abundance analysis. For this highly altered sample, the octovertet ratio is no longer efficient to distinguish phases. It is likely due to the homogenization of the composition created by the redistribution of elements during alteration (see Discussion). The different metallic and mineral phases are distinguished with respect to the intensity of the Fe, S and Ni signals (Figure 6). On the scale of the intensity of the Fe signal the range of intensity for each phase is indicated. To get a unique description of a phase, it appears to be necessary to give also its range of intensity on the S and Ni maps as well in order to, for example, discriminate kamacite, low-Ni kamacite and intermediate S phases. Using the IDL software, we get the number of pixels which fulfills the intensity conditions for each phase. The study of a 14

mm^2 area of GRO 95577 (Table 5) indicates that in chondrule, vermiculite accounts for 25.2 area% and clinochlore mesostasis for 13.2 area%. Opaque phases are represented by low-Ni kamacite 2.3 area%, kamacite 0.2 area%, pyrrhotite accounts for 1.1 area%, whereas intermediate sulfide phases account for 5.0 area% and magnetite for 1.1 area%. Ca-rich carbonates account for 6.4 area%, while the Fe-rich phyllosilicates matrix is the most important fraction with 45.6 area%.

DISCUSSION

A precise modal analysis method

The modal analysis method based on the study of X-ray elemental maps acquired on the electron microprobe provides a new more precise modal analysis of Renazzo and GRO 95577. Up to now, for CR chondrites, only the proportion of chondrules, opaque phase and matrix have been reported in literature. Bland et al. (2004) and Menzies et al. (2005) were the first ones to feel the necessity to find an alternative to the existing modal analysis methods. Methods based on normative abundances recalculated from chemical analyses or on point counting are limited when the sample is fine-grained. Thus Bland et al. (2004) and Menzies et al. (2005) defined a new-modal analysis method which combines the use of X-ray diffraction and Mössbauer spectroscopy. They are able to assess the presence of minerals having abundance above 1 wt% from the analysis of a few hundreds of micrograms. But their technique has the limitation that it requires an extensive database of minerals standards in order to deconvolve complex X-ray patterns.

Our method requires the use of a polished or thin section, but enables computation of the area% of each mineral phase. There is no limitation except that the investigator should have already a good knowledge of the mineralogy of the sample. The conversion of area% to volume% is a point however, which deserves further discussion. Usually, according to the literature, the crystals are supposed to be prismatic so that the vol% equals the area%. The opposite attitude would be to consider crystals as uniform spheres so that vol% equals $(\text{area}\%)^{3/2}$. Because of this uncertainty, the vol% are given in Table 5 for both cases a) considering prismatic crystals and b) considering spherical crystals. The results are compared to the available data on CRs which are for prismatic crystals only. The influence of this form factor is illustrated when comparing the distribution 4.9 vol% of opaque phases, 47.9 vol% of matrix and 46.4 vol% of chondrule for prismatic crystals with the distribution 1.4 vol% of opaque phases, 61.4 vol% of matrix and 37.1 vol% of chondrule for spherical crystals. For future work, one may consider combining CT tomography with the elemental determination. In such instances, the shape of minerals and their chemistry would be available to calculate a very realistic %vol. It will then be necessary to re-evaluate several meteorites in order to update the literature data. But, for now, because the literature data are established by considering vol%=area%, we are discussing the results established for this case a).

New data on Renazzo and GRO 95577

This study provides an updated description of the mineralogy of Renazzo and GRO 95577. Particular attention was given to the description of the phyllosilicates as well as the sulfide phases, which are of a particular interest when studying the aqueous alteration processes.

Concerning Renazzo, our mineralogical description is in agreement with previous studies (Table 1 to Table 3) and gives new information concerning the composition of the pyroxenes, the feldspathic mesostasis and the sulfide phases. Concerning the modal abundances, Smith et al. (2004) and Weisberg et al. (2003) indicate respectively 6.1 vol% - 8.1 vol% for opaque

phases, 41.4 – 41.9 vol% for matrix and 49.6 - 51.1 vol% for chondrule. Our data (Table 5), 4.9 vol% for opaque phases, 47.9 vol% for matrix and 46.4 vol% for chondrule, are within the same range as previous data except for matrix, which is a bit higher. Moreover, we observed that the feldspathic mesostasis vol% is higher than the chamosite mesostasis vol%, which reveals that the aqueous alteration in Renazzo was not so strong.
Concerning GRO 95577, the compositions of chondrule, mesostasis and opaque phases given by Weisberg and Prinz (2000) were revised (Table 2 to Table 4 and Table 6). There was no data available data in literature concerning its modal abundances but the modal distribution we established (Table 5) falls within the CR range. Both the qualitative and quantitative studies allow us to discuss GRO 95577 as a CR1.

CR1 status of GRO 95577 confirmed by qualitative and quantitative description

Weisberg et al. (1993) stated that GRO 95577 is a CR1 having an oxygen isotopic composition ($\delta^{18}O$=6.32‰, $\delta^{17}O$=2.83‰), which plots close to Renazzo ($\delta^{18}O$=6.25‰, $\delta^{17}O$=2.29‰) in the three oxygen isotope diagram (Figure 7). Thanks to the present study more information are available to confirm the CR1 status of GRO 95577.
The modal analysis of GRO 95577 states that its opaque phases, matrix and chondrule abundances fall within the CR range. The characteristics of GRO 95577 are compared to the CR key-properties (Weisberg et al. 1993) in Table 7 and it appears that there is a good match except for the presence of Fe-Ni metal and olivine-pyroxene in chondrules. This non-adequation is due to the high degree of alteration in GRO 95577 which turns these Fe-Ni metal and olivine-pyroxene respectively in low-Ni kamacite, magnetite and in vermiculite. Up to now, neither microchondrule in matrix nor Amaeboid Olivine Aggregate (AOA) has been reported and the ^{15}N isotopic composition of GRO 95577 is not yet available.
As mentioned above, in GRO 95577, forsteritic olivine, augite and orthopyroxene have been totally replaced by vermiculite. This illustrates an extremely high degree of aqueous alteration, as even in CM1s or in very altered CM2, such as Nogoya (Zolensky et al. 1993; Hanowski and Brearley 2001, Brearley 2006), and in Orgueil CI1 (Bland et al. 2004) this replacement is only partial. Thus, the abundance of Ca-carbonates, the presence of magnetite and intermediate sulfide phases as well as the lack of anhydrous minerals support the petrologic type 1 described by Weisberg and Prinz (2000). This petrologic type 1 is slightly different to the typical one described by Van Schmus and Wood (1967) and Sears and Dodd (1988) because the outlines of the chondrules are still visible as it was already observed in the rounded relict chondrules in CM1 clasts in Kaidun for example (Zolensky et al. 1996).

The alteration phases in CR1 chondrite

For CRs, Zolensky et al. (1993) reported aqueous alteration phases as being silicates such as Fe-Mg serpentines and saponite, oxides such as magnetite, sulfides such as pyrrhotite and pentlandite and a minor amount of carbonates such as calcite. The present study of GRO 95577 shows that its alteration phases, except Ca-carbonates, are not the classic ones. These are vermiculite and chlorite (clinochlore) for the silicates, and intermediate sulfide phases.
Chlorite and vermiculite were reported by Zolensky et al. (1993) as minor fine-grained phase in CMs. Intermediate sulfide phases are described as being rare in CR2 microclasts of the Y 793497 howardite (Gounelle et al. 2003) but they are more abundant in CM2 microclasts in Kapoeta howardite (Zolensky and Di Valentin 1998; Gounelle et al. 2003) which is consistent with the presence of these intermediate sulfide phases in CM chondrites (Scott and Taylor 1985; Alexander et al. 1989; Zolensky and Thomas 1995; Chokai et al. 2004).

This underlines the existence of a wider range of conditions for the aqueous alteration of CRs as well as some similarities between CR and CM alteration processes.

Wide range of aqueous alteration on CR parent-body

The primitive CR2 chondrites, MET 00426, EET 99177 (Abreu and Brearley 2005, 2006), EET 92042 (Busemann et al. 2006), the moderately altered CR2 Renazzo and the extremely hydrated CR1 GRO 95577, display a very wide range of aqueous alteration for CR chondrites.

One way to illustrate it is to consider the chemical composition of the very common alteration products, the phyllosilicates. The composition of the phyllosilicates in the chondrule and in the matrix of Renazzo and GRO 95577 are plotted in (Mg, Fe, Si+Al) ternary diagrams respectively in Figure 4 and Figure 8. Only data obtained by using focused beam analyses are represented.

The composition of the phyllosilicates in the chondrules of Renazzo and GRO 95577 are compared to the ones from other CR2s (Al Rais and Y 790112 in Weisberg et al. 1993), from CR2 microclasts in Kapoeta howardite (Gounelle et al. 2003), from CV3s (Allende, Vigarano, Bali, Kaba in Zolensky et al. 1993), from CM2s (EET 83389, Bells, Y 791198, Murchison, Cochacamba, Nogoya, Mighei, Murray, MAC 88101, LEW 88001, Y 793321, B 7904, Y 86720 in Bunch and Chang (1980) and in Zolensky et al. (1993)), from CM2 microclasts in Kapoeta howardite (Gounelle et al. 2003) and from CM1s (EET 83334 and ALH 88045 in Zolensky et al. 1993). The composition of the vermiculite from GRO 95577 cores and the clinochlore from the GRO 95577 mesostasis plot at the low-iron pole of the composition field of the phyllosilicates in CR cores. The closest composition is the one of the Mg-serpentine in the chondrule core of the Nogoya CM2 chondrite (Bunch and Chang 1980).

The composition of the phyllosilicates in the matrix are compared to the ones from the CR-CV3 chondrites, NWA 1152 and SAH 00182 (in Smith et al. 2004), from CR2 (EET 87770 in Zolensky et al. 1993), from CR2 microclasts (in Y 793497, Jodzie and Kapoeta howardites in Zolensky et al. 1996 and Gounelle et al. 2003), from CV3s (Allende, Vigarano, Bali and Kaba in Bunch and Chang 1980 and Zolensky et al. 1993), from CM2s (ALH 83100, EET 83389, Bells, Y 791198, Murchison, Cochamba, Nogoya, Mighei, LEW 85307, MAC 88107, ALH 83016, ALH 84029, Murray, LEW 87148, ALHA 81002, MAC 88101, LEW 88001, Y 793221, B 7904, Y 86720 in Bunch and Chang 1980 and Zolensky et al. 1993), from CM1s (EET 83334, Y 82042 in Zolensky et al. 1993) and from CI1 (Ivuna, Orgueil, Alais and Y 82162 in Kerridge 1976, Tomeoka and Buseck 1988, Zolensky et al. 1993). The composition field defined by phyllosilicates in the matrix of CR2s and CR1 (GRO 95577) is more restricted than the one defined by the phyllosilicates in CM2s and CM1s matrices. “Renazzo” plots at the Fe-rich end of the range whereas “GRO 95577” plots at the Fe-poor end. The composition of phyllosilicates in GRO 95577 matrix plots close to the ones in the matrix of the much altered CM2 Nogoya (Zolensky et al. 1993), of the CI1 Orgueil (Tomeoka and Buseck 1988) and in CR2 microclast in Jodzie howardite (Zolensky et al. 1996).

The compositions of the phyllosilicates in the chondrule and in the matrix of GRO 95577 are coherent with a high degree of aqueous alteration. Indeed, this phenomenon produces iron-poor phyllosilicates such as those found in the highly hydrated CM2 Nogoya chondrite. Browning et al. (1996) introduced a mineralogical alteration index (MAI) based on the Fe^{3+}/Si ratio in the phyllosilicates from the matrix of CM falls. This index evolves with the increasing degree of aqueous alteration. As an example, on the ternary diagram (Figure 8), the evolution of the composition from the one of the serpentine in CM Murray chondrites (Fe-rich pole) to the one of Nogoya phyllosilicates (Fe-poor pole) on the elliptic field of

composition of CMs phyllosilicates is explained by an increasing degree of aqueous alteration. GRO 95577 has numerous similarities with the highly altered CM2 chondrite, Nogoya, as their phyllosilicates in chondrules and in matrix have about the same plot in the (Mg, Fe, Si+Al) ternary plots. Moreover these two chondrites both contain clinochlore as well as intermediate sulfide phases.

The composition of the phyllosilicates from the matrix in the two CR-CV3, NWA 1152 and SAH 00182 (Smith et al. 2004) (Figure 8) are coherent with the one of other CV3s (Bunch and Chang 1980; Zolensky et al. 1993). Their location on the diagram at the Fe-pole of the CR trend is logical considering their anhydrous mineralogy. On contrary, the fact that the compositions of phyllosilicates in CM1s (EET 83334 and Y 82042 in Zolensky et al. 1993) plot in the middle of the CM range does not correspond to the trend. On the solely argument of the phyllosilicates composition in the matrix, EET 83334 and Y 82042 are not CR1.

The fact that the composition field of phyllosilicates in CRs is more restricted than for CMs can be interpreted as a result of a better homogeneity of the mineralogy of the parent-body, notably the repartition of kamacite and sulfide which are the source of iron for phyllosilicates, and/or to more restricted physico-chemical conditions of aqueous alteration.

With the increasing aqueous alteration there is a decrease in iron content in phyllosilicates but there is also a modification of the bulk matrix composition, which is apparent when comparing Renazzo (CR2) and GRO 95577 (CR1) (Table 4). Renazzo's matrix is richer in FeO and SO3 whereas GRO 95577's matrix is richer is MgO and SiO_2.

In Renazzo's matrix, iron and sulfur must rather be considered in term of Fe and S than in term of FeO and SO_3. Indeed, in Renazzo matrix, S is within pyrrhotite. In GRO 95577 Fe and S are not in matrix but are incorporated within intermediate sulfide phases preferentially located at the border or within chondrules as evidenced on the X-ray maps of GRO 95577 (Figure 6). These phases are quoted 5 and are in green on the Fe map, in red on the S map and in green to red on the Ni map. So, a transfer of Fe and S is likely occurring from the matrix to the chondrules during the aqueous alteration process. Grossman (2002) has already described this phenomenon as the sulfur content in matrix decreases and the abundance of sulfides in chondrules increases with the increasing degree of alteration, in the order Graves Nunataks (GRA) 95229 – Renazzo – Al Rais. Similarly to what we observe in GRO 95577, Grossman indicates that sulfides replace metal grains, especially near chondrule surfaces. The Al Rais matrix composition (McSween and Richardson 1977) is compared to Renazzo and GRO 95577 ones in Table 4. On contrary to what Grossman (2002) states, we do not observe the lower S-content in Al Rais matrix than in Renazzo one. This is another illustration of the anomalous status of Al Rais within the CRs (Kallemeyn 1993).

The greater abundance of MgO and SiO2 in GRO 95577's matrix than in Renazzo one is coherent with the observations of McSween (1979, 1987) when studying the composition of CMs matrix. According McSween, prior to the aqueous alteration, the CM chondrites can, simplistically, be regarded as consisting of a mixture of Fe-rich fine-grained matrix and Mg-rich chondrules. McSween (1979, 1987) predicts that with progressive alteration, matrix should become more Mg-rich and chondrules more Mg-depleted and that the extent of this alteration is linked to brecciation. But as noted by Brearley (2006), more recent studies show that advanced aqueous alteration can also occur entirely independent of brecciation. It is obvious when considering the relatively heavily altered CM chondrites, such as ALH 81002 and several CM1 chondrites that are essentially unbrecciated (Llorca and Brearley 1992; Zolensky et al. 1997; Hanowski and Brearley 2001). This latter point is confirmed by the observation of the GRO 95577 CR1 sample in which no evidence of brecciation is observable, as the outlines of its chondrules are still well defined, although it is heavily

altered. It is interesting to note that in terms of MgO, SiO, FeO and SO3, the composition of Orgueil matrix (CI) is intermediate between this of Renazzo and GRO 95577 (Table 4).

Confirmation of a possible relationship between Renazzo and GRO 95577

In order to test whether the alteration of Renazzo could result in a GRO 95577-like composition, the elemental compositions of these two chondrites were calculated and are reported in Table 8. To calculate these compositions, the modal analysis (Table 5) and the mineralogical composition of each component (Table 1 to Table 6) are used as input data. The following hypotheses are made:

- Ca-carbonates in Renazzo and GRO 95577 are assumed to be calcite;
- densities of kamacite, low-Ni kamacite and intermediate S phases are calculated by balancing the density of Fe, Ni and S with respect to their abundances in these phases;
- in Renazzo, the density of the matrix is assumed to be the one of a mixture of 75% of forsterite and 25% of fayalite, the density of the olivine is assumed to be the one of forsterite, the one of pyroxene is assumed to be the one of enstatite and the one of the feldspathic mesostasis is assumed to be the one of anorthite;
- in GRO 95577, the density of the matrix is assumed to be similar to the one of antigorite or clinochlore.

It is thus possible to compute the elemental repartition (wt% for 1 m^3) in these two chondrites (Table 8). The elemental repartition of Renazzo is compared to the one obtained by chemical analysis by Mason and Wiik (1962) after having recalculated this one in order to avoid H, N, V, Cu. Table 8 indicates that there is a good match between these two repartitions. It is very important since it stresses the accuracy of our mineralogical description and modal analysis method as well as the relevance of the hypotheses concerning the densities of minerals.
The differences between the element repartition in GRO 95577 and the average repartition in Renazzo is also reported in Table 8. A great similarity exists between these two repartitions. There is only a discrepancy of 3 wt% of Mg and 4 wt% of Si and an excess of 5 wt% of S and 2 wt% of Ca in GRO 95577 compared to Renazzo. These differences are low and favor the idea that it is possible that the CR2 Renazzo-like composition is altered into a CR1 GRO 95577-like composition via an isochemical process, except for the H_2O input.

Characteristics of the aqueous alteration process of Renazzo into GRO 95577

When considering the mineralogy and texture of Renazzo and GRO 95577, different constraints on the mechanism of alteration from a CR2 chondrite to the CR1 chondrite can be made.

The texture and the outlines of chondrules are preserved in GRO 95577 (Weisberg and Prinz (2000)). This implies that the alteration process is mostly a chemical process rather than a mechanical one. No evidence of brecciation is observed. This suggests that the heat may mostly originate from the decay of ^{26}Al (Urey 1955) rather than from accretion processes and favors the idea that alteration occurred after the accretion of the parent-body.

Moreover, when considering the mineralogy and the chemical composition of Renazzo and GRO 95577 other conclusions can be made. The elemental repartition in Renazzo and GRO 95577 (Table 8) supports the existence of an isochemical alteration process turning the CR2 composition into the CR1 one. Such isochemical process is reported for the carbonaceous chondrite parent body by e.g. Clayton and Mayeda (1984), Wulf et al. (1995) and Bland et al. (2006). Moreover, in Renazzo, most of the chondrules consist of forsteritic olivine (Fo_{99}),

pyroxene and a feldspathic mesostasis, which means Si, Mg, Al and Ca are the major elements. In GRO 95577, chondrules consist of vermiculite and clinochlore mesostasis, which means, Si, Mg, Al and Fe in composition. So, vermiculite may result from the aqueous alteration of olivine, pyroxene (sources of Si, Mg) and feldspathic mesostasis (source of Al), and from the corrosion of the blebs of metal (source of Fe). The aqueous alteration of the feldspathic mesostasis provides Ca which is incorporated in the Ca-carbonate observed in GRO 95577. Carbon may come from the aqueous alteration of the organic matter present in Renazzo's matrix or from an input in CO_2. Moreover the feldspathic mesostasis in Renazzo may be enriched in Mg coming from the alteration of the adjacent olivine and pyroxene and in Fe coming from the blebs of metal. By this mean its composition evolves into clinochlore as observed in GRO 95577. The Fe, S rich matrix in Renazzo turns into a Mg, Si rich one in GRO 95577. This is due to the migration of Fe and S up to the chondrule interiors where these elements react with FeNi metal to turn into intermediate sulfide phases. Regarding these considerations and the elemental repartitions in Renazzo and GRO 95577, the aqueous alteration can be regarded as an isochemical process except for the supply in H_2O and for the possible input in CO_2. This alteration creates the migration of chemical elements (mostly Fe, Ni, S, Al, Mg and C) at a millimeter to centimeter scale, which favors the idea of an alteration on the parent body. In Renazzo, Ca-carbonates are mostly observed at the border between matrix and chondrules. Hutchison et al. (1987) made the same observation for Bishunpur (unequilibrated ordinary chondrite) and attributed it to the fact that the margin of chondrules may represent a sink for Ca that has been mobilized from mesostasis by aqueous fluids. This argument supports also the hypothesis of an aqueous alteration occurring on the parent-asteroid. Finally, the fact that the magnetite and phyllosilicates separates from Renazzo have O isotopic compositions that lie on the terrestrial fractionation line indicates that they come from the same fluid (Clayton and Mayeda 1977) which is also most compatible with alteration within an asteroidal environment (Clayton and Mayeda 1999).

These conclusions are coherent with the one of Weisberg et al. (1993) favoring the asteroidal location of the aqueous alteration for CRs but it must not be ignored that some textural evidences in the Y 8449 CR2 chondrite (Ichikawa and Ikeda 1995) make the existence of some preaccretionary alteration possible as well.

The composition of the unaltered CR parent asteroid

From the modal analysis of Renazzo (Table 5) and from the information we have on the chemical reactions which occur during the aqueous alteration, it is possible to estimate the composition of Renazzo prior to the alteration. This composition is called the unaltered CR composition.

It is considered that prior to the aqueous alteration:

- FeNi metal was kamacite only;
- S was only in the matrix;
- the core of the chondrule consisted in olivine and pyroxene;
- the mesostasis was feldspathic in composition;
- there was no calcite and C was in the matrix while Ca was in the feldspathic mesostasis.

After the aqueous alteration, for 1 m^3, in term of mass of element (g) :

- $(Fe_{kamacite})$unaltered CR = $(Fe_{kamacite} + Fe_{low\text{-}Ni\ kamacite} + Fe_{chamosite})$Renazzo (1);
- $(Al_{felspathic\ mesostasis})$unaltered CR = $(Al_{chamosite} + Al_{felspathic\ mesostasis})$Renazzo (2);
- (S_{matrix})unaltered CR = $(S_{matrix} + S_{intermediate\ S\ phases})$Renazzo (3);
- (Fe_{matrix})unaltered CR = $(Fe_{matrix} + Fe_{intermediate\ S\ phases})$Renazzo (4);

- (C_{matrix})unaltered CR = $(C_{matrix} + C_{calcite})$Renazzo (5);
- for the other elements E, (E_{matrix})unaltered CR = (E_{matrix})Renazzo (6).

Kamacite is partly altered into low-Ni kamacite thus liberating Fe, which is available for the conversion of the feldspathic mesostasis into chamosite mesostasis (1) and (2). The sulfide phases in matrix are partly altered liberating Fe and S, which is available to combine with Ni (coming from the alteration of kamacite) and result in the crystallization of intermediate sulfide phases (3) and (4). The organic matter in matrix is partly altered into Ca-carbonate (5). Knowing the mass of Fe in kamacite of the unaltered CR chondrites, $(Fe_{kamacite})$unaltered CR , it is possible to compute the elemental composition of the kamacite, by applying proportionality to the elemental composition of the kamacite in Renazzo. The same method is used to compute the elemental composition of the feldspathic mesostasis in the unaltered CR from the mass $(Al_{felspathic\ mesostasis})$unaltered CR. The composition of the matrix in the unaltered CR (Table 4) equals the one of Renazzo at which the amount of S and Fe from the intermediate sulfide phases and the amount of C from calcite are added. The proportions of olivine and pyroxene are supposed to be the same than in Renazzo.

Knowing the density of kamacite (7.84), of the matrix (estimated to be 3.55), of the feldspathic mesostasis (2.76) and of olivine and pyroxene (3.21), the modal abundances in the unaltered CR are calculated. Thus the CR unaltered body is estimated to have 4 vol% of kamacite whose composition is the same than in Renazzo (Table 3), 50 vol% of matrix whose composition is in Table 4, and 46 vol% of chondrule (19.5 vol% of olivine, 23 vol% of pyroxene, 3.5 vol% of feldspathic mesostasis, all having the same composition than in Renazzo).

CONCLUSIONS

The use of EMP X-ray elemental maps and a crystal chemistry approach facilitated with IDL software reveal a new method to achieve the modal analysis of a sample. It requires having a good knowledge of the mineralogical composition of the sample, but one can achieve the modal analysis of a 1 mm^2 map in about 4 hours which is much faster and more convenient than by using the point counting method. By this mean, new data on CR chondrites were collected and resulted in new insights concerning their aqueous alteration process.

First of all, we refined the classification of Renazzo and GRO 95577. The majority of the mesostasis in Renazzo is feldspathic rather than chamosite so it favors the idea that this meteorite is not as highly altered as reported in literature. We support the previous classification of GRO 95577, as a CR1.

Moreover, the homogeneity of GRO 95577 phyllosilicates composition, their low Fe-content, and the distinctive matrix composition of Renazzo and GRO 95577 require a wide range of aqueous alteration within CRs. New alteration products for CR chondrites are even found in GRO 95577, vermiculite, clinochlore and intermediate S phases, which underlines similarities with the highly altered CM2 chondrite, Nogoya.

The preservation of the outlines of the chondrules in GRO 95577 and the elemental transfers of Al, Fe and Ca throughout the chondrule and of Fe, S from the matrix to the chondrule support an asteroidal aqueous alteration.

From the mineralogical data and modal abundances in Renazzo and GRO 95577, it was possible to compute the elemental repartition in these two chondrites. The results indicate that the aqueous alteration is isochemical except for the input of H_2O.

From the modal analysis of Renazzo and from the information we have on the chemical reactions occurring during the aqueous alteration, it is possible to compute the composition of Renazzo prior to the alteration. The modal abundances in an unaltered CR are thus estimated

to be 4 vol% of kamacite, 50 vol% of matrix and 46 vol% of chondrule (19.5 vol% of olivine, 23 vol% of pyroxene, 3.5 vol% of feldspathic mesostasis).

In upcoming articles, it will be shown how the results of the modal analysis are used by modeling works to put more constraints on the physico-chemical conditions which prevail during the aqueous alteration. Then, these parameters will themselves be used for hydrothermal aqueous alteration experiments on synthetic unaltered CR mineralogical assemblages, whose reaction products will be compared to the mineralogy of GRO 95577. By this means we could test whether our hypotheses concerning the evolution of a Renazzo-like material into GRO 95577-like material are pertinent or not.

Acknowledgments. The authors would like to thank the National Research Council (NRC) and Oak Ridge Associated Universities (ORAU) NASA Postdoctoral Programs which granted this research. Dr M. E. Zolensky was supported by NASA's Cosmochemistry program. Many thanks also to the Meteorite Working Group (MWG at NASA-JSC) and to the Museum National d'Histoire Naturelle de Paris who provided us respectively with chips of GRO 95577 and Renazzo thick section.

REFERENCES

Abreu N. M., and Brearley A. J. 2005. Mineralogical characterization of the matrices of the primitive CR chondrites MET00426 and EET99177 (abstract #5332). *Proceedings of the 68th METSOC meeting*.

Abreu N. M., and Brearley A. J. 2006. Early solar system processes recorded in the matrices of CR2 chondrites MET 00426 and QUE 99177 (abstract #5372). *Proceedings of the 69th METSOC meeting*.

Alexander C. M. O. D., Barber D. J., and Hutchison R. 1989 The microstructure of Semarkona and Bishunpur. *Geochimica et Cosmochimica Acta* 53:3045-3057.

Alexander C. M. O. D., Russell S. S., Arden J.W., Ash R.D., Grady M. M. and Pillinger C. T. 1998. The origin of chondritic macromolecular organic matter: A carbon and nitrogen isotope study. *Meteoritics & Planetary Science* 33:603-622.

Ash R. D., Morse A. D., and Pillinger C. T. 1993. The survival of presolar organic material in CR chondrites? *Meteoritics* 28:318.

Bayliss P. 1975. Nomenclature of the trioctahedral chlorites. *Canadian Mineralogist* 13 :178-180.

Bischoff A., Palme H., Schultz L., Ash R. D., Clayton R. N., Herpers U., Stoffler D., Grady M. M., Pillinger C. T., Spettel B., Weber H., Grund T., Endreb M. and Weber D. 1993 a. Paired Renazzo-type (CR) carbonaceous chondrites from the Sahara. *Geochimica et Cosmochimica Acta* 57:1587-1603.

Bischoff A., Palme H., Ash R. D., Weber D., Weber H. and Spettel B 1993 b. Acfer-182 and paired samples, an iron-rich carbonaceous chondrite – similarities with ALH 85085 and relationship to CR chondrites. *Geochimica et Cosmochimica Acta* 57:2631-2648.

Bland P. A., Cressey G., and Menzies O. N. 2004. Modal mineralogy of carbonaceous chondrites by X-ray diffraction and Mössbauer spectroscopy. *Meteoritics & Planetary Science* 39:3-16.

Brearley A. J. 2006. The action of water. In Meteorites and the Early Solar System II (eds. Lauretta D. S., and McSween Jr. H.). The University of Arizona Press, Tucson, in collaboration with Lunar and Planetary Institute, Houston. 943 p.

Browning L. B., Mc Sween Jr. H., and Zolensky M. E. 1996. Correlated alteration effects in CM carbonaceous chondrites. *Geochimica et Cosmochimica Acta* 60:2621-2633.

Bunch T. E., and Chang S. 1980. Carbonaceous chondrites: II Carbonaceous chondrite (CM) phyllosilicates and light element geochemistry as indicators of parent-body processes and surface conditions. *Geochimica et Cosmochimica Acta* 44:1543-1577.

Busemann H., Alexander C. M. O'd., Nittler, L. R., Zega, T. J., Stroud, R. M., Cody, G. D., Yabuta, H., and Hoppe, P. 2006. Correlated microscale isotope and scanning transmission X-ray analyses of isotopically anomalous organic matter from the CR2 Chondrite EET 92042 (abstract #2005). 36th Lunar and Planetary Science Conference.

Caillere S., Henin S., and Rautureau M. 1982 Minéralogie des argiles, classification et nomenclature, 2nd ed. Paris : Masson. 189 p.

Chokai J., Zolensky M. E., Le L., Nakamura K., Monkawa A., Koizumi E., and Miyamoto M. 2004. aqueous alteration mineralogy in CM carbonaceous chondrites. (abstract #1506). 35th Lunar and Planetary Science Conference.

Clayton R. N., and Mayeda T. K. 1977. Oxygen isotopic compositions of separated fractions of the Leoville and Renazzo carbonaceous chondrites. *Meteoritics* 12:199.

Clayton R. N., and Mayeda T. K. 1984. The oxygen isotope record in Murchison and other carbonaceous chondrites. *Earth and Planetary Science Letters* 67: 151-166.

646 Clayton R. N., and Mayeda T. K. 1999. Oxygen isotope studies of carbonaceous chondrites
647 *Geochimica et Cosmochimica Acta* 63:2089-2104.
648 Connolly Jr. H. C., Huss G. R., and Wasserburg G. J. 2001. On the formation of Fe-Ni metal
649 in Renazzo-like carbonaceous chondrites. *Geochimica et Cosmochimica Acta* 65:4567-
650 4588.
651 Fredriksson K., Mason B., Beauchap R., and Kurat G. (1981) carbonates and magnetites in
652 the Renazzo chondrites. *Meteoritics* 16:316.
653 Gounelle M., Zolensky M. E., Liou J. -C., Bland P. A., and Alard O. 2003. Mineralogy of
654 carbonaceous chondritic microclasts in howardites: identification of C2 fossil
655 micrometeorites. *Geochimica et Cosmochimica Acta* 67:507-527.
656 Grossman J. N. 2002. The redistribution of sulfides during metamorphism and aqueous
657 alteration of primitive chondrites (abstract #5158). *Proceedings of the 65th METSOC*
658 *meeting*.
659 Hanowski N. P., and Brearley A. J. 2001. Aqueous alteration of chondrules in the CM
660 carbonaceous chondrites, Allan Hills 81002. *Geochimica et Cosmochimica Acta*
661 65:495-518.
662 Hutchison R., Alexander C. M. O., and Barber D. J. 1987. The Sermakona meteorite: first
663 recorded occurrence of smectite in an ordinary chondrite and its implications.
664 *Geochimica et Cosmochimica Acta* 51:1875-1882.
665 Ichikawa O., and Ikeda Y. 1995. Petrology of the Yamato-8449 CR chondrite. *Proceedings of*
666 *the NIPR Symposium on Antarctic Meteorites* 8:63-78.
667 Kallemeyn G. W. 1993. The Al Rais meteorite: a CR chondrites or close relative? (abstract
668 #747). 24th Lunar and Planetary Science Conference.
669 Kallemeyn G. W., and Wasson J. T. 1982 The compositional classification of chondrites. III
670 – Ungrouped carbonaceous chondrites. *Geochimica et Cosmochimica Acta* 46: 2217-
671 2228.
672 Kolodny Y., Kerridge J. F., and Kaplan I. R. 1980. Deuterium in carbonaceous chondrites;
673 *Earth and Planetary Science Letters* 46: 149-158.
674 Kung C. C., and Clayton R. N. 1978. Nitrogen abundances and isotopic compositions in
675 stony meteorites. *Earth and Planetary Science Letters* 38: 421-435.
676 Lee M. S., Rubin A. E., and Wasson J. T. 1992. Origin of metallic Fe-Ni in Renazzo and
677 related chondrites. *Geochimica et Cosmochimica Acta* 56: 2521-2533.
678 Llorca J., and Brearley A. J. 1992 Alteration of chondrules in ALH 84034 an unusual CM2
679 carbonaceous chondrite (abstract #793). *23rd Lunar and Planetary Science Conference*.
680 Mason B. 1997. GRO 95577. *Antarctic Meteorite News Letter* 20:10-11.
681 Mason B., and Wiik H. B. 1962. The Renazzo meteorite. American Museum Novitates 2106:
682 1-11.
683 McSween H. Y. 1977. Petrographic variations among carbonaceous chondrites of the
684 Vigarano type. *Geochimica et Cosmochimica Acta* 41:1777-1790.
685 McSween H. Y. Jr 1979. Alteration in CM carbonaceous chondrites inferred from modal and
686 chemical variations in matrix. *Geochimica et Cosmochimica Acta* 43:1761-1770.
687 McSween H. Y. Jr 1987. Aqueous alteration in carbonaceous chondrites: mass balance
688 constraints on matrix mineralogy. *Geochimica et Cosmochimica Acta* 51:2469-2477.
689 McSween H. Y. Jr, and Richardson S. M. 1977. The composition of carbonaceous chondrite
690 matrix. *Geochimica et Cosmochimica Acta* 41:1145-1161.
691 Menzies O. N., Bland P. A., Berry, F. J., and Cressey G. 2005. A Mössbauer spectroscopy
692 and X-ray diffraction study of ordinary chondrites : Quantification of modal
693 mineralogy and implications for redox conditions during metamorphisms. *Meteoritics*
694 *& Planetary Science* 40:1023-1042.

695 Nelen J., Kurat G., and Fredriksson K 1975. The Renazzo chondrite – A reevaluation.
696 *Meteoritics* 10: 464-465.
697 Noguchi T. 1995. Petrology and mineralogy of the PCA 91082 chondrite and its comparison
698 with the Yamato-793495 (CR) chondrite. *Proceedings of the Symposium on Antarctic*
699 *meteorites* 8:241-255.
700 Pearson V. K., Sephton M. A., and Gilmour I. 2006. Molecular and isotopic indicators of
701 alteration in CR chondrites. *Meteoritics & Planetary Science* 41: 1291-1303.
702 Schwandt C. S., Jones J. H., Mittlefehldt D. W., and Treiman A. H. (2001) The magma
703 composition of EET79001A: The First Recount (abstract #1913). *32nd Lunar and*
704 *Planetary Science Conference*.
705 Schwandt C. S., and McKay, G. (2005) Element ration maps: A more informative use of
706 digital elemental X-ray maps than single element maps. *Proceedings Microscopy and*
707 *Microanalysis 2005, 1300 CD*.
708 Schwandt C. S. (2006a) Petrogenesis clues: Complex chemical zoning within the pyroxenes
709 of martian meteorites, Eos Trans. *AGU*, 87(36), Jt. Assem. Suppl., MB52A-05.
710 Schwandt C.S. (2006b) Crystal chemistry inspired element ratio mapping improves the
711 understanding of petrogenesis: Martian meteorite examples. *Microscopy and*
712 *Microanalysis*, 12, Suppl. 2, 820CD.
713 Scott E. R. D., and Taylor G. J. 1985. Petrology of types 4-6 carbonaceous chondrites.
714 *Proceedings of the NIPR Symposium on Antarctic Meteorites* 9:699-709.
715 Sears D. W. G., and Dodd R. T. (1988). Overview and classification of meteorites. In
716 Meteorites and the Early Solar System (eds. Kerridge J. F. and Matthews M. S.), The
717 University of Arizona Press, Tucson :3-31.
718 Smith C. L., Russel S. S., Gounelle M., Greenwood R. C., and Franchi, I. A. 2004. NWA
719 1152 and Sahara 00182: new primitive carbonaceous chondrites with affinities to the
720 CR and CV groups. *Meteoritics & Planetary Science* 3: 2009-2032.
721 Tomeoka K. and Buseck P. R. 1988. Matrix mineralogy of the Orgeuil CI carbonaceous
722 chondrite. *Geochimica et Cosmochimica Acta* 52:1627-1640.
723 Urey H. C. 1955. The cosmic abundances of potassium, uranium, and thorium and the heat
724 balances of the Earth, the Moon and Mars. *Proceedings of the National Academy of*
725 *Sciences U. S.* 41: 127-144.
726 Van Schmus R., and Wood J. A.1967. A chemical-petrologic classification for the chondritic
727 meteorites. *Geochimica et Cosmochimica Acta* 31:747-765.
728 Weisberg M., Prinz M., Clayton R. N., and Mayeda T. K 1993. The CR (Renazzo-type)
729 carbonaceous chondrite group and its implications. *Geochimica et Cosmochimica Acta*
730 57:1567-1586.
731 Weisberg M. K., Prinz M., Clayton R. N., Mayeda T. K., Grady M.M., and Pillinger C.T.
732 1995. The CR chondrite clan. *Proceedings of the NIPR Symposium on Antarctic*
733 *Meteorites* 8:11-32.
734 Weisberg M., and Prinz M. 2000. The Grosvenor Mountains 95577 CR1 chondrite and
735 hydration of the CR chondrites (abstract #5154). *Proceedings of the 63rd METSOC*
736 *meeting*.
737 Wood J. A. 1967. Chondrites: their metallic minerals, thermal histories, and parent planets.
738 *Icarus* 6:1-49.
739 Wulf A. V., Palme H., Jochum K. P. 1995. Fractionation of volatile elements in the early
740 solar system: evidence from heating experiments on primitive meteorites. *Planetary*
741 *and Space Sciences* 43:451-468.
742 Zanda B., Bourot-Denise M., and Perron C. 1991. Cr, P and Si in the metal of Renazzo
743 (abstract #1543). *22th Lunar and Planetary Science Conference*.

744 Zolensky M. E., Bourcier W. L., and Gooding J. L. 1989. Aqueous alteration on the hydrous
745 asteroids: Results of EQ3/6 computer simulations. *Icarus* 78:411-425.
746 Zolensky M. E. 1991. Mineralogy and matrix composition of CR chondrites Renazzo and
747 EET 87770 and ungrouped Essebi and MAC 87300. *Meteoritics* 21:414.
748 Zolensky M. E, Barrett R., and Browning L. 1993. Mineralogy and composition of matrix
749 and chondrule rims in carbonaceous chondrites. *Geochimica et Cosmochimica Acta*
750 57:3123-3148.
751 Zolensky M. E., and Browning L. B. 1994. CM chondrites exhibit the complete petrologic
752 range from 2 to 1. *Meteoritics* 29: 556.
753 Zolensky M. E., and Thomas K. L. 1995. Iron and iron nickel sulfides in chondritic
754 interplanetary dust particles. *Geochimica et Cosmochimica Acta* 59: 4707-4712.
755 Zolensky M. E., Ivanov A. V., Yang V., Mittlefehldt D. W., Ohsumi K. 1996. The Kaidun
756 meteorite: mineralogy of an unusual CM1 lithology. *Meteoritics & Planetary Science*
757 *31*: 484-493.
758 Zolensky M. E., Weisberg M. K., Buchanan P. C., and Mittlefehldt D. W. 1996. Mineralogy
759 of carbonaceous chondrites clasts in HED achondrites and the Moon. *Meteoritics &*
760 *Planetary Science* 31: 518-537.
761 Zolensky M. E., Mittlefehldt D. W., Lipschutz M. E., Wang M-S., Clayton, R. N., Mayeda T.
762 K. Grady M. M., Pillinger C. T., and Barber D. 1997. CM chondrites exhibit the
763 complete petrologic range from type 2 to 1. *Geochimica et Cosmochimica Acta* 61:
764 5099-5115.
765 Zolensky M. E., Di Valentin T. 1998. Iron-nickel sulfides as environmental indicators for
766 chondritic materials. *Proceedings of the NIPR Symposium on Antarctic Meteorites*
767 23:183-185.

TABLES

Table 1. Representative analyses (in wt%) of silicates within Renazzo chondrules.

Na_2O	MgO	Al_2O_3	SiO_2	P_2O_5	K_2O	CaO	TiO_2	Cr_2O_3	FeO	MnO	Total	
						Olivine						
n.d.	56.03	0.21	42.42	n.d.	n.d.	0.37	n.d.	0.18	0.75	0.03	99.96	Fo_{99}[1]
n.d.	55.20	n.d.	42.00	n.d.	n.d.	0.10	n.d.	0.30	1.80	0.10	99.50	Fo_{98}[2]
n.d.	56.70	n.d.	40.30	n.d.	n.d.	0.32	n.d.	0.20	1.29	0.07	98.88	Fo_{99}[3]
						Fe olivine						
n.d.	32.53	0.18	37.09	n.d.	n.d.	0.34	n.d.	0.25	29.12	0.45	99.99	Fo_{66}[1]
n.d.	31.40	n.d.	36.20	n.d.	n.d.	0.20	n.d.	0.50	30.70	0.90	99.99	Fo_{64}[2]
						Pyroxene						
0.05	35.72	3.69	54.91	n.d.	n.d.	0.64	1.55	1.07	2.08	0.25	99.96	Fs_4Wo_1[1]
0.06	29.43	3.7	54.47	n.d.	n.d.	5.15	0.77	1.44	4.55	0.41	99.98	Fs_8Wo_{10}[1]
0.04	21.5	6.11	52.35	n.d.	n.d.	15.29	0.8	1.44	2.18	0.31	100.02	Fs_4Wo_{33}[1]
n.d.	38.00	0.60	57.90	n.d.	n.d.	0.30	n.d.	0.70	1.90	n.d.	99.40	Fs_3Wo_1[2]
n.d.	37.20	1.54	57.80	n.d.	n.d	0.51	0.18	0.93	2.31	0.17	100.64	Fs_3Wo_1[3]
0.05	36.10	0.83	57.10	n.d.	n.d.	0.33	0.08	0.68	3.10	0.16	98.43	Fs_4Wo_1[3]

[1]: this study. [2]: in Nelen et al. (1975). [3]: in Weisberg et al. (1993).

773

774 Table 2. Representative analyses (in wt%) of the mesostasis within Renazzo and GRO 95577 chondrules.

	Na_2O	MgO	Al_2O_3	SiO_2	P_2O_5	K_2O	CaO	TiO_2	Cr_2O_3	FeO	MnO	Total	
Feldspar													
Renazzo	0.39	n.d.	35.99	46.72	n.d.	n.d.	16.90	n.d.	n.d.	n.d.	n.d.	100.00	An_{96}[1]
Chamosite													
Renazzo	n.d.	8.35	12.28	30.30	n.d.	n.d.	1.05	n.d.	n.d.	31.91	0.37	84.26	[1]
Renazzo	0.31.	11.50	15.10	29.10	n.d.	0.06.	0.76	0.30	0.23	32.70	0.36	90.40	[2]
Clinochlore													
GRO 95577	n.d.	17.21	14.99	30.18	n.d.	n.d.	0.13	n.d.	n.d.	21.19	0.53	84.22	Clin. 1[1]
GRO 95577	n.d.	19.08	14.23	31.33	n.d.	n.d.	0.49	n.d.	n.d.	19.48	0.45	85.07	Clin. 2[1]
Serpentine													
Renazzo	n.d.	16.0	4.50	39.30	n.d.	n.d.	0.40	n.d.	0.10	20.70	0.20	81.00	[2]

775 [1]: this study. [2]: in Nelen et al. (1975). [3]: in Weisberg et al. (1993).

776

777 Table 3. Representative analyses (in wt%) of opaque phases within Renazzo and GRO 95577.

	Si	P	S	Ti	Cr	Mn	Fe	Co	Ni	Total
Kamacite										
Renazzo[1]	0.20	0.35	0.22	0.25	0.32	0.19	88.9	0.14	9.44	100.00
Renazzo[2]	n.d.	0.05-0.62	n.d.	n.d.	0.13-0.73	n.d.	83.4-93.3	0.17-0.55	5.8-13.8	
GRO 95577[1]	0.02	0.12	0.02	0.01	0.31	n.d.	86.25	0.54	12.73	99.99
Low-Ni kamacite										
Renazzo[1]	0.17	0.44	0.19	0.2	0.3	0.18	93.61	0.08	4.85	100.00
GRO 95577[1]	0.37	0.22	1.21	0.09	0.43	0.07	94.05	0.17	3.38	100.00
Pyrrhotite										
GRO 95577[1]	0.13	n.d.	36.01	n.d.	0.04	0.02	63.30	0.01	0.45	99.96
Intermediate sulfide phases										
GRO 95577[1]	2.13	0.03	33.65	0.01	0.14	0.03	51.66	0.63	11.7	99.99
Pentlandite										
GRO 95577[1]	0.11	0.31	36.86	0.16	0.2	0.26	32.57	0.91	28.64	100.02

778 [1]: this study. [2]: in Weisberg et al. (1993)

779

780 Table 4. Representative analyses (in wt%) of the matrix within some CRs and Orgueil. From computation for the unaltered CR body.

	Na_2O	MgO	Al_2O_3	SiO_2	SO_3	K_2O	CaO	TiO_2	Cr_2O_3	FeO	MnO	NiO	Total
Renazzo[1]	n.d.	14.0	3.0	30.20	8.74	n.d.	2.30	0.30	0.30	24.80	0.20	1.90	85.74
Renazzo[2]	1.16	15.80	2.66	31.40	7.94	0.16	0.87	0.07	0.35	24.30	0.33	1.48	86.52
Renazzo[3]	0.78	16.63	3.07	34.62	5.99	0.10	0.61	0.06	0.31	27.47	0.23	2.14	92.01
Average Renazzo	1.55	15.48	2.91	32.07	7.56	0.13	1.26	0.14	0.32	25.52	0.25	1.84	89.03
Average Renazzo for total=100%	1.74	17.39	3.27	36.02	8.49	0.15	1.42	0.16	0.36	28.66	0.28	2.07	100.00
GRO 95577[4]	1.23	30.78	3.13	43.05	5.67	0.18	0.80	0.26	0.50	14.17	0.23	n.d.	100.00
Al Rais for total=100%[3]	1.25	19.3	2.71	33.71	9.48	0.17	1.69	0.08	0.41	28.23	0.22	2.73	100.00
Unaltered CR body[4]	1.66	16.62	3.12	34.42	10.58	0.14	1.36	0.15	0.34	29.34	0.27	1.98	99.98
Orgueil[3]	0.05	19.79	2.57	32.99	3.30	0.02	0.29	0.08	0.58	22.28	0.26	2.78	84.99
Orgueil for total=100%	0.06	23.29	3.02	28.82	3.88	0.02	0.34	0.09	0.68	26.21	0.31	3.27	100.00

781 [1]: in Nelen et al. (1975). [2]: in McSween and Richardson (1977). [3]: in Zolensky et al. (1993). [4]. this study. EMPA analyses with defocused beam
782 for [1], [2] and [3] and FESEM focused beam for GRO 95577 [4].

Table 5. Modal abundances of mineral and metallic phases within Renazzo and GRO 95577. Comparison to data on CRs from Smith literature. Computation of the modal abundances within the CR unaltered body (see text for details).

	Renazzo vol%				GRO 95577 vol%		CRs vol%	Unaltered CR vol%
	[1]a	[1]b	[2]a	[3]a	[1]a	[1]b	[2-3]a	[1]a
Kamacite	0.7	0.1			0.2	≈0		4
Low-Ni kamacite	3.3	1.1			2.3	0.7		0
Magnetite	0	0			1.1	0.2		0
Pyrrhotite	0	0			1.1	0.2		0
Intermediate S phases	0.9	0.2			5.0	2.2		0
Total opaque phases	4.9	1.4	6.1	8.1	9.7	3.3	4.8-10.2	4
Matrix	47.9	61.4	41.9	41.4[4]	45.6	59.7	29.7-63	50
Olivine	19.2	15.5			0	0		19.5
Pyroxene	23.0	20.4			0	0		23
Vermiculite	0	0			25.2	24.6		0
Feldspathic mesostasis	2.8	0.8			0	0		3.5
Chamosite mesostasis	1.4	0.3			0	0		0
Clinochlore mesostasis	0	0			13.2	9.3		0
Total chondrule	46.4	37.1	51.1	49.6	38.4	33.9	37-63.1	46
Ca-carbonate	0.8		0.1		6.4	3.1		0

[1]: this study. [2]: in Smith et al. (2004). [3]: in Weisberg et al. (1993). [4]: includes dark inclusions. a) for prismatic crystals hypothesis, vol%=area%, b) for spherical crystals hypothesis, vol%=(area%)$^{3/2}$.

788

789 Table 6. Representative analyses of silicates (in wt%) within GRO 95577 chondrules.

Na_2O	MgO	Al_2O_3	SiO_2	P_2O_5	K_2O	CaO	TiO_2	Cr_2O_3	Fe_2O_3	MnO	Total
Vermiculite (Fe_2O_3)											
1.22	32.79	2.91	45.23	n.d.	0.16	0.25	n.d.	0.96	16.48	n.d.	100.00

790

791 Table 7. Adequation between the key-properties for CRs chondrites and GRO 95577 mineralogy.

Key properties for CR chondrites [1]	In GRO 95577 [2]
1. Chondrules	
• large, up to 5 mm with a mean size of 1mm	Yes
• multilayered;	Yes
• Fe-Ni metal rich;	Altered
• type I that have olivine and/or pyroxene-rich cores with layers of olivine/pyroxene, serpentine, Fe-Ni metal and Ca-carbonate	Altered
2. Abundant matrix and dark inclusions that contain	
• microchondrules and microfragments (<200 μm)	N/A
• magnetite framboids and platelets	Yes
3. Unique assemblage of hydrous silicates	
• chlorite-rich chondrule mesostases	Yes
• serpentine-rich rims	Yes
• serpentine-rich brown microspheres on chondrule margins, in chondrule rims and in the matrix	N/A
4. Ca-carbonates are different from those of other groups in composition. Moreover there are Ca-carbonate rims on chondrules which do not exist in other group	Yes
5. Abundant Fe,Ni metal have a positive Ni vs Co trend with a solar ratio	N/A
6. The abundance of refractory inclusions is low	Yes
7. AOAs have both Mn-rich and Mn-poor forsterite	N/A
8. There is a unique CR mixing line on the three oxygen isotope diagram, whose slope is 0.7AOAs have both Mn-rich and Mn-poor forsterite	Yes
9. CRs are enriched in ^{15}N AOAs have both Mn-rich and Mn-poor forsterite	N/A

792 1. in Weisberg et al. 1993. 2. this study. N/A : not observed.

793 Table 8. Elemental repartition (wt% in $1m^3$) of Renazzo and GRO 95577. Comparison to Mason and Wiik (1962) data on Renazzo. See
794 Discussion for details.

C	Na	Mg	Al	Si	P	S	K	Ca	Ti	Cr	Mn	Fe	Co	Ni	
n.s.	1	25	3	29	n.s.	4	n.s.	2	n.s.	1	n.s.	34	n.s.	1	Renazzo[1]
2	1	23	2	25	n.s.	2	n.s.	2	n.s.	1	n.s.	39	n.s.	2	Renazzo[2]
1	1	21	3	23	n.s.	8	n.s.	4	n.s.	1	n.s.	36	n.s.	2	GRO 95577[1]
≈	≈	-3	≈	-4	≈	5	≈	2	≈	≈	≈	-0.5	≈	0.5	GRO 95577 – average Renazzo
n.s.	1	25	3	29	n.s.	4	n.s.	2	n.s.	1	n.s.	34	n.s.	1	Unaltered CR body[1]

795 1. this study. 2. Mason and Wiik (1962). n.s. not significant.
796

FIGURES

Figure 1

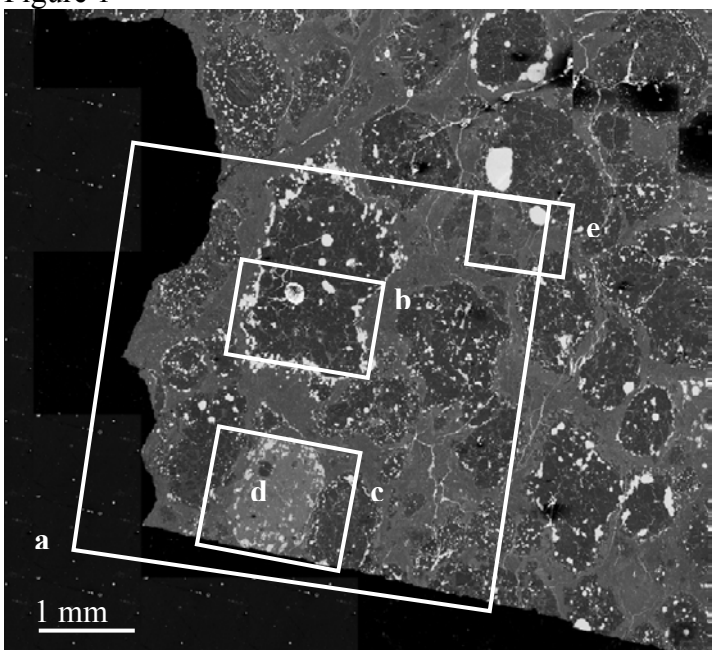

802 Figure 1a

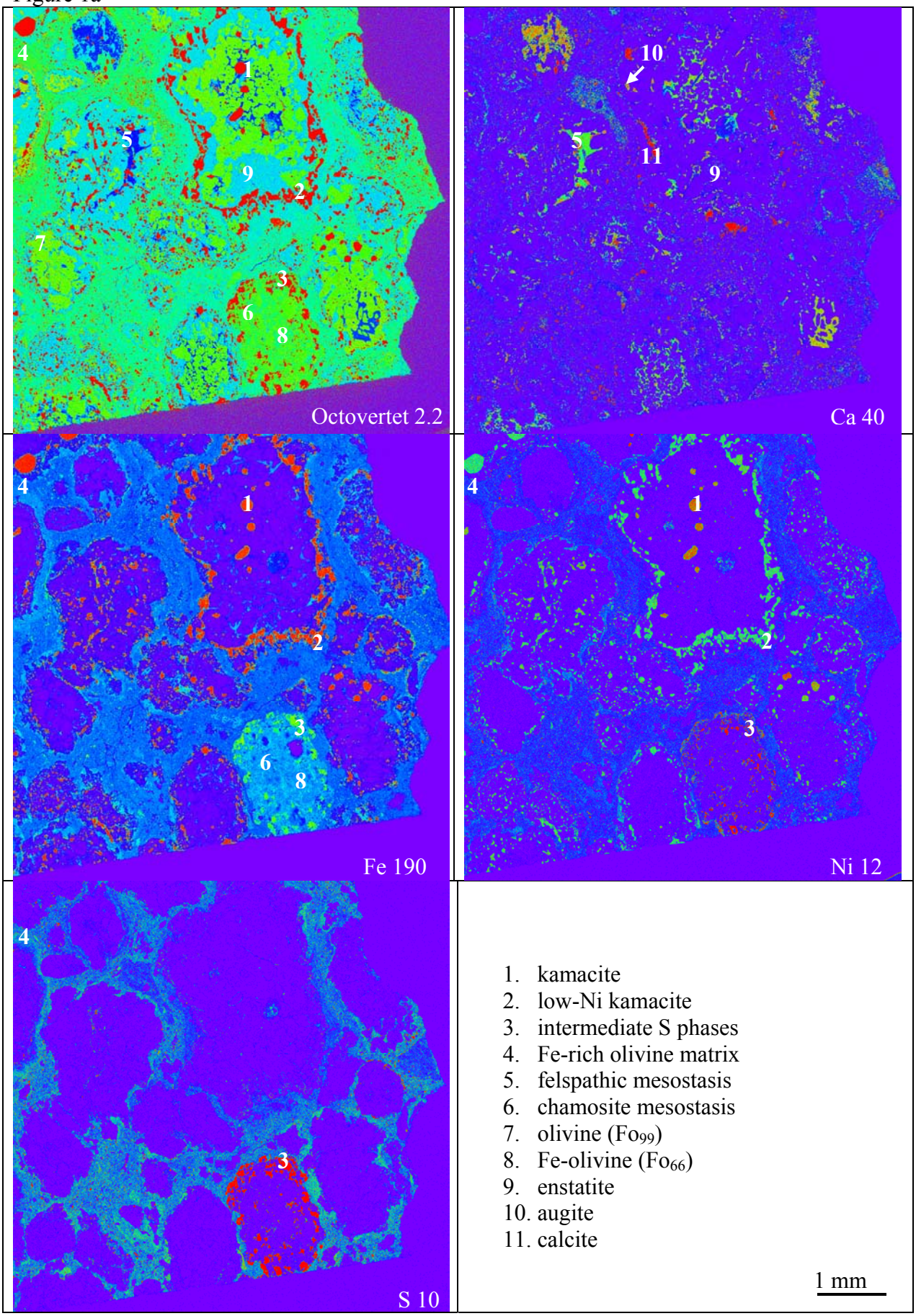

803
804 Figure 1b

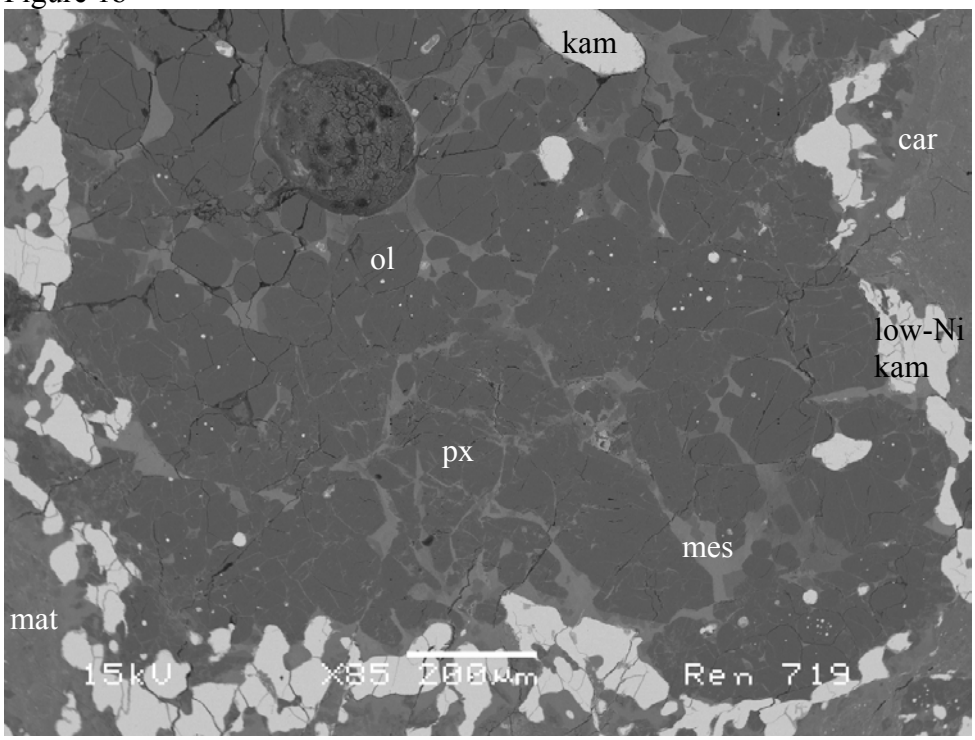

805
806
807 Figure 1c

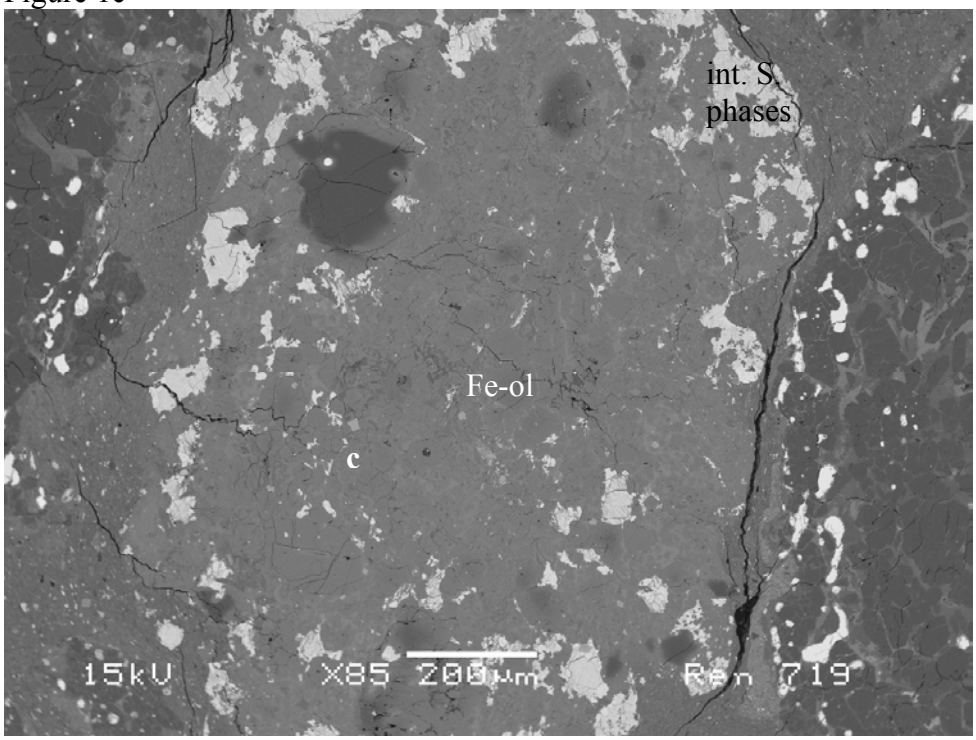

808

809
810 Figure 1d

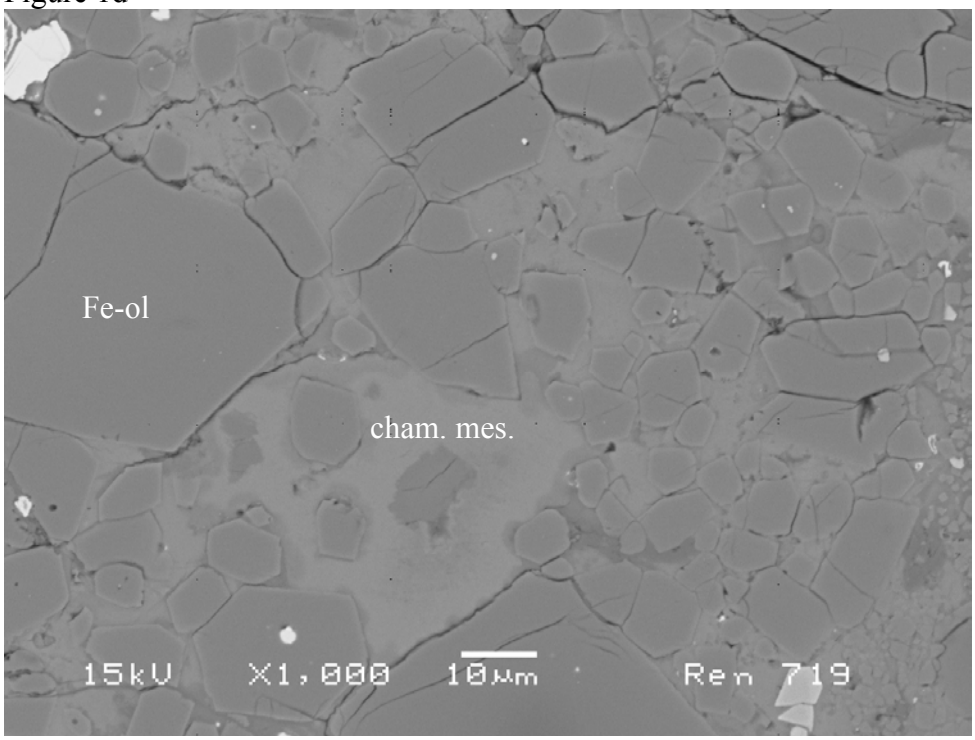

811
812
813 Figure 1e

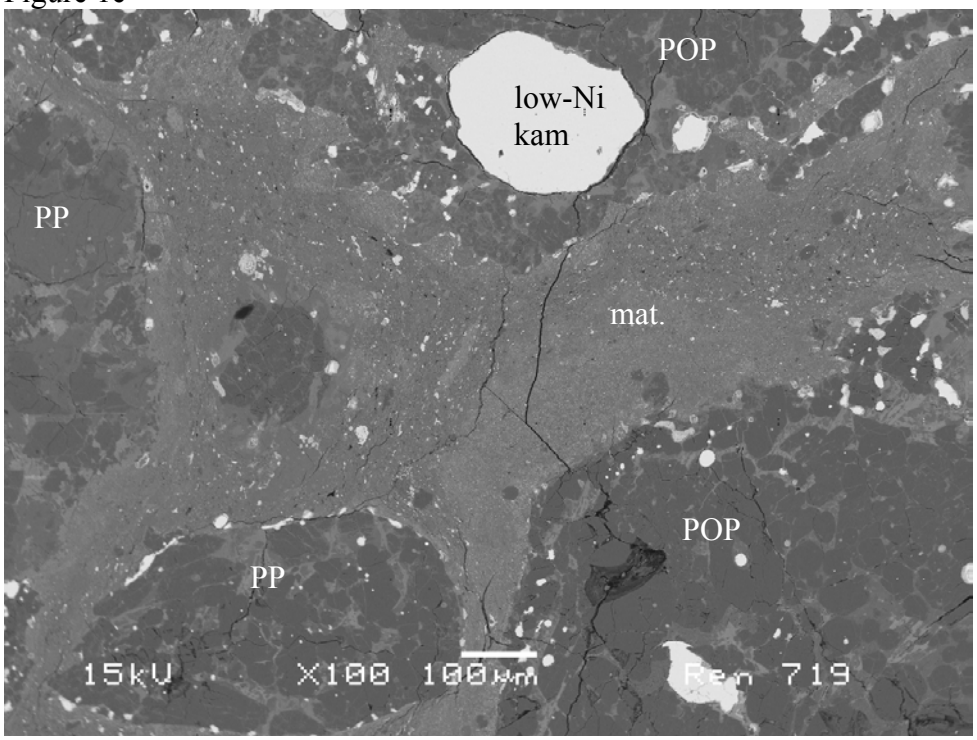

814

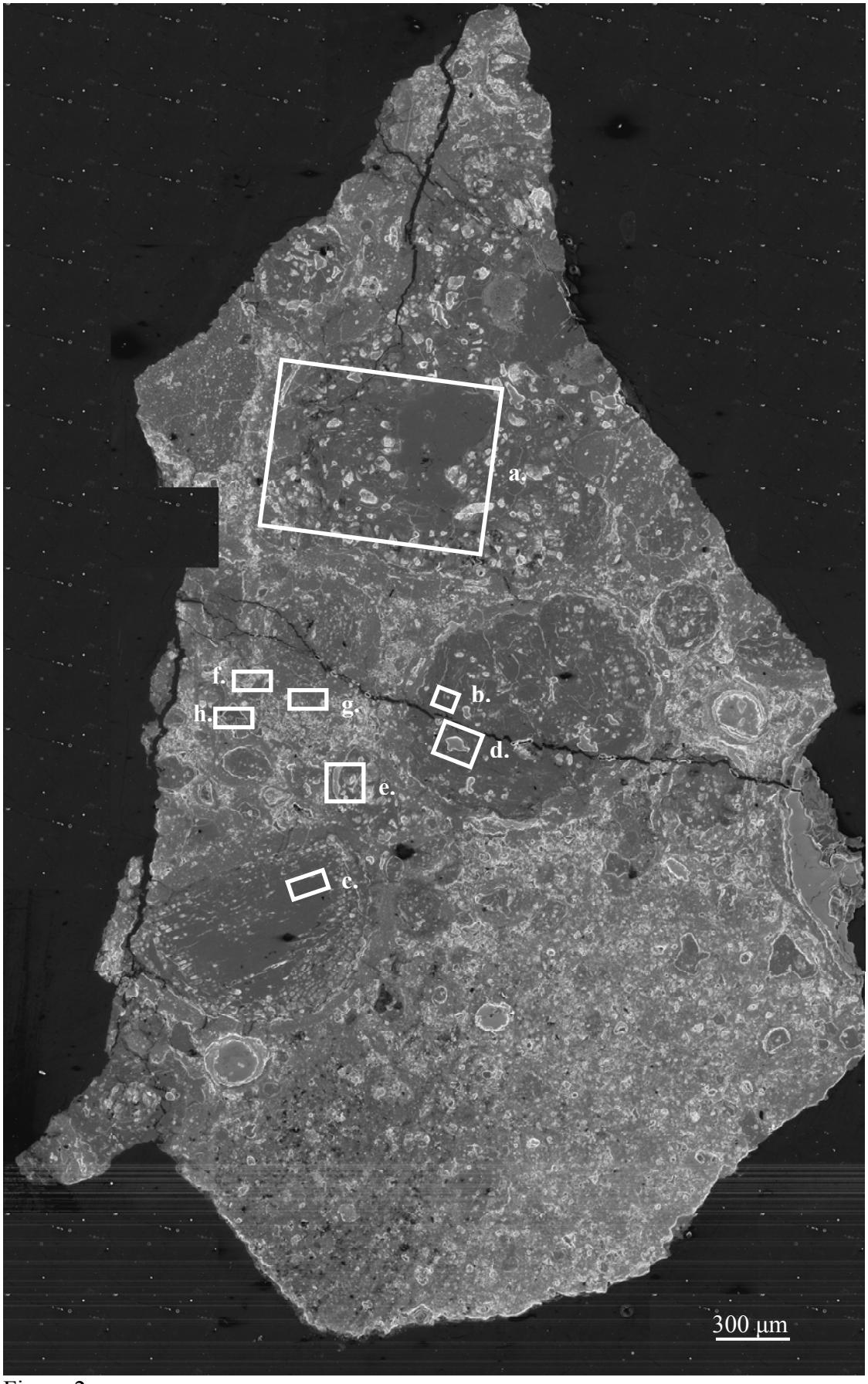

Figure 2

820 Figure 2a.

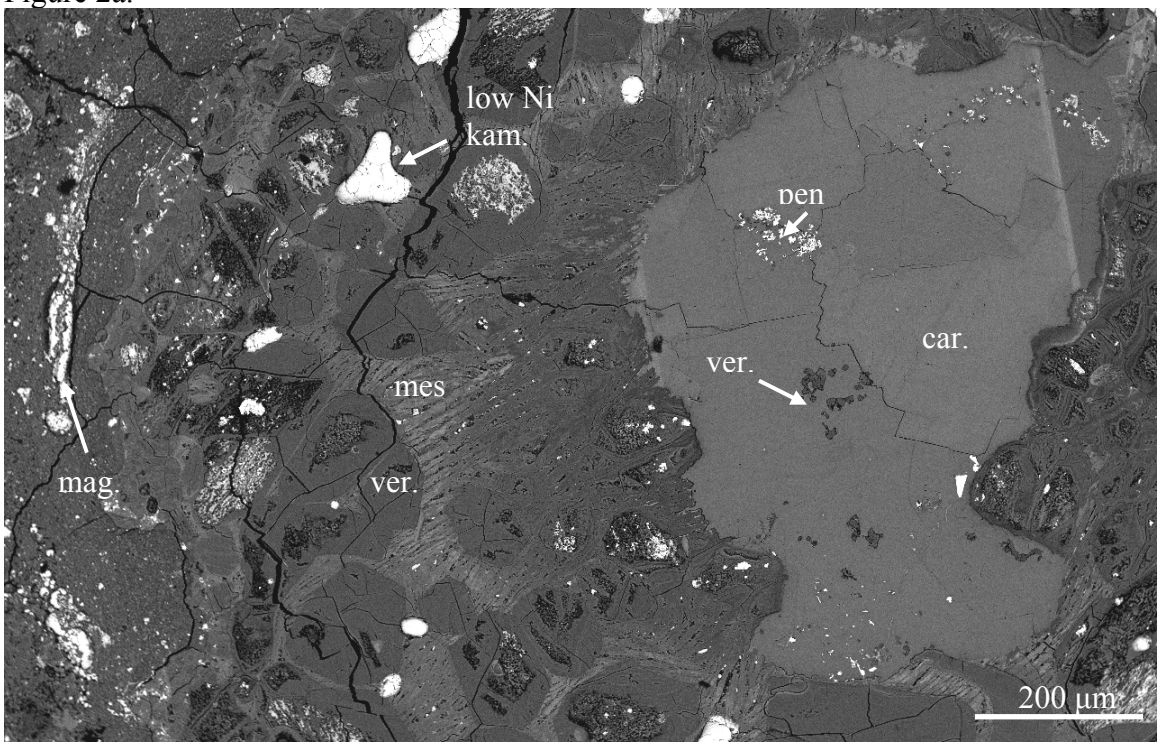

821
822
823 Figure 2b.

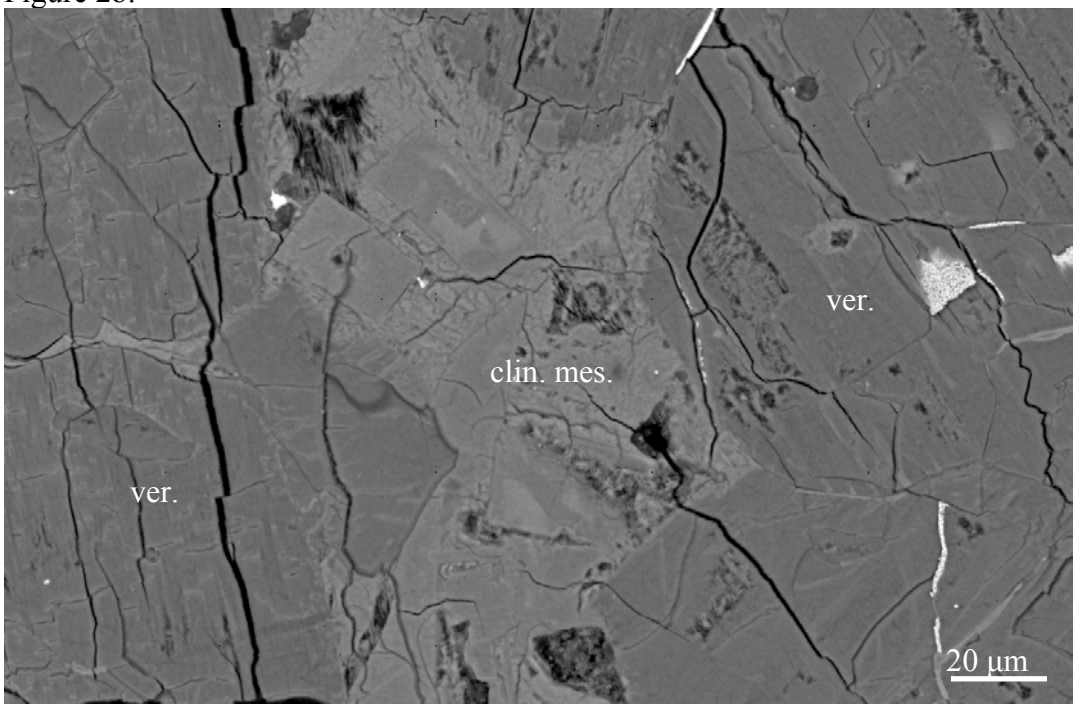

824

825 Figure 2c.

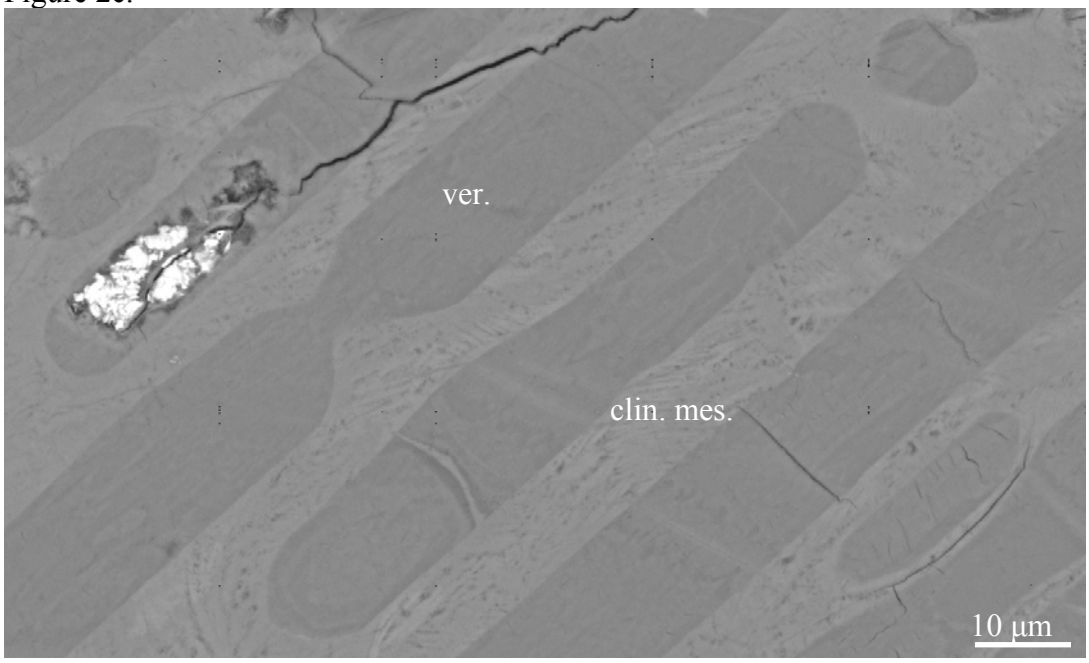

826
827
828 Figure 2d.

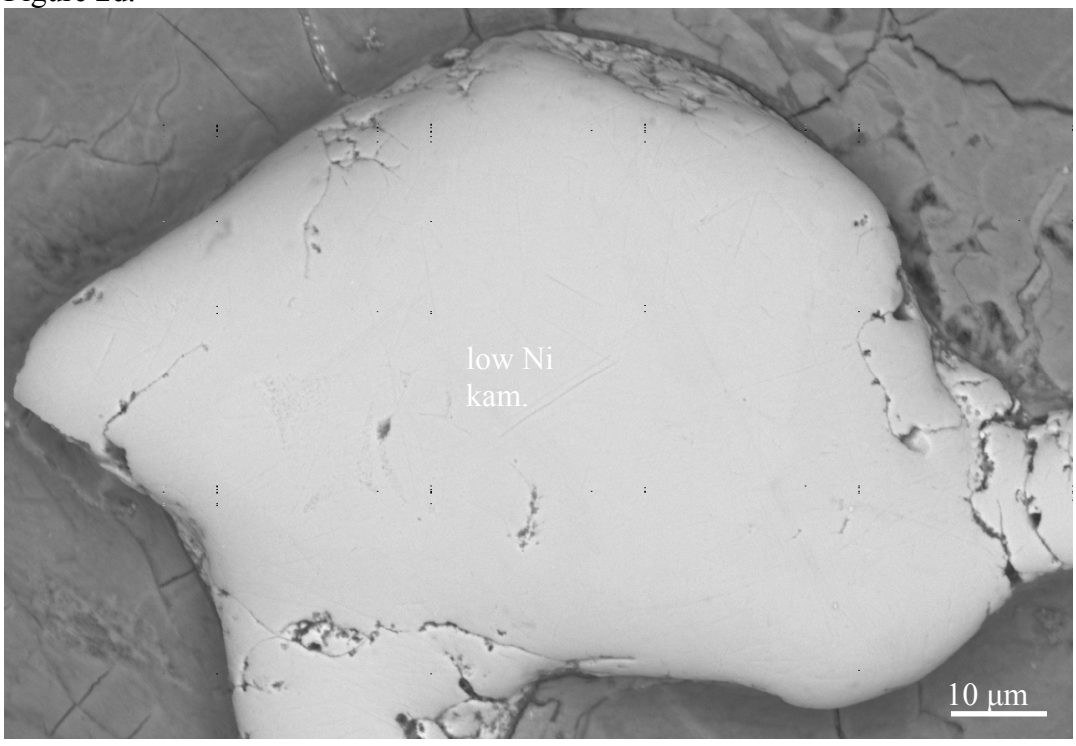

829

Figure 2e.

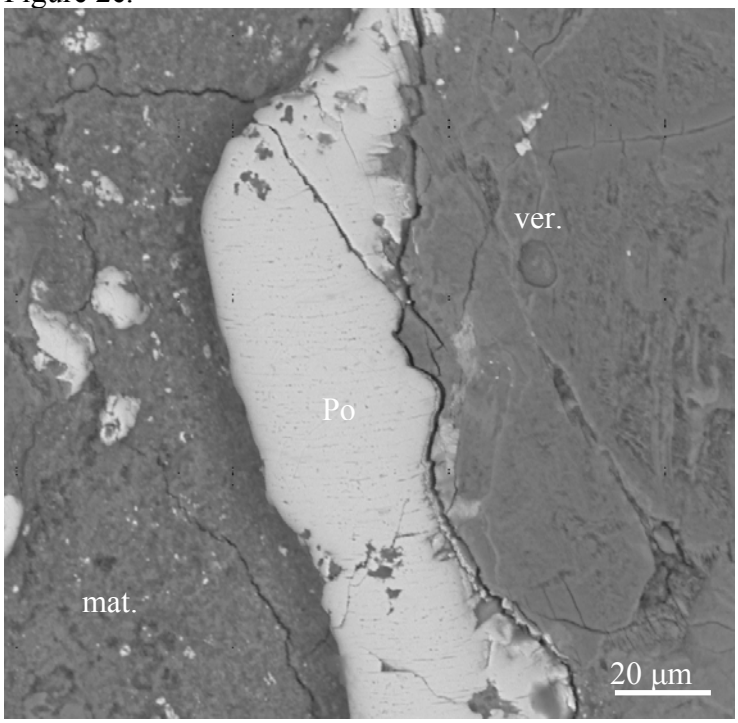

Figure 2f.

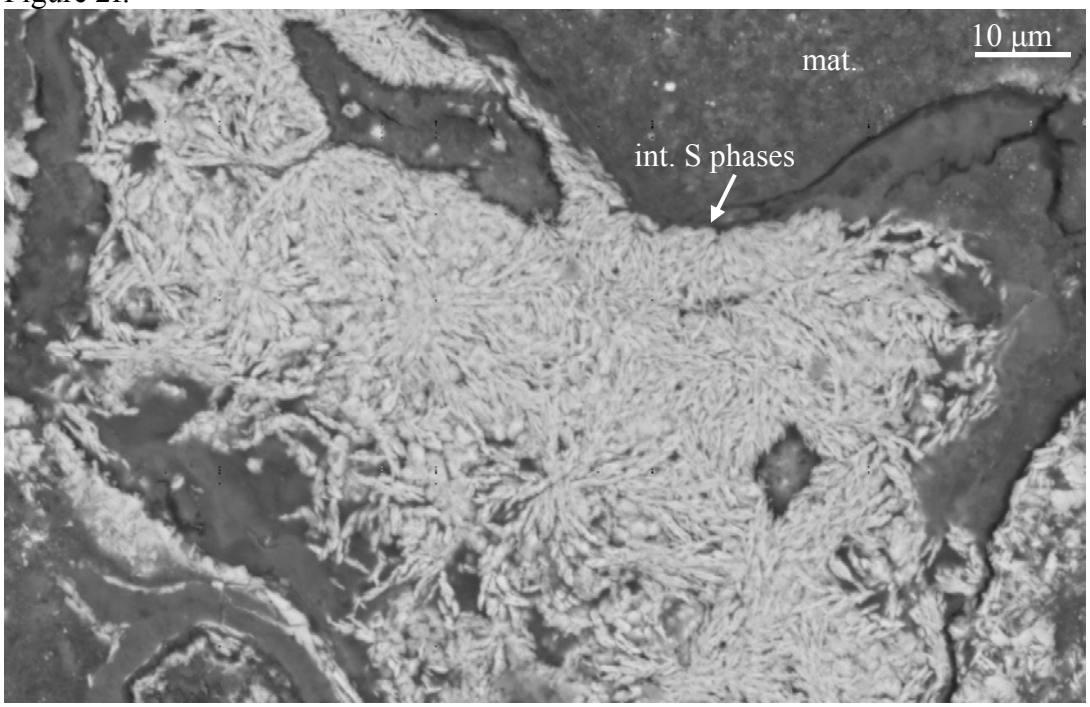

Figure 2g.

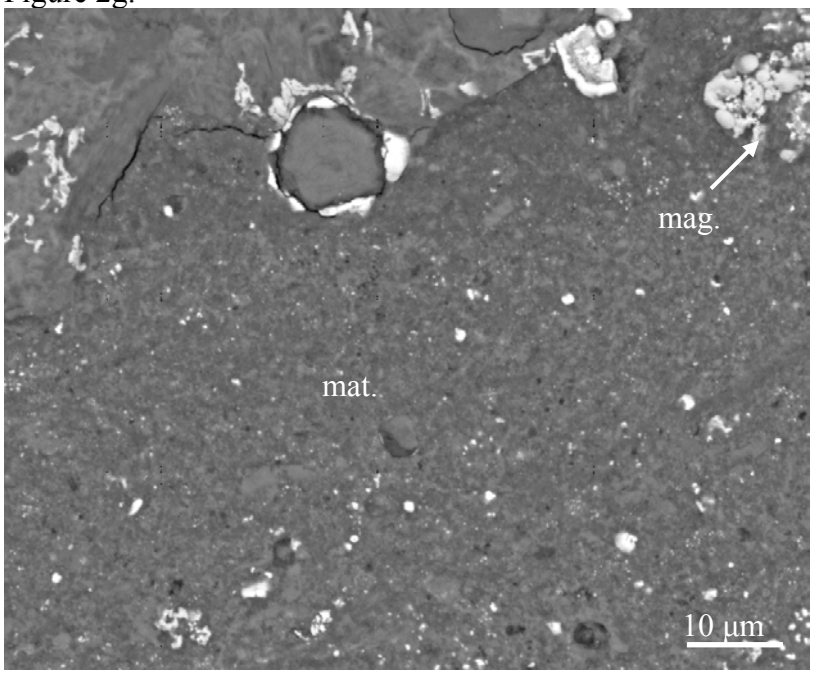

Figure 2h.

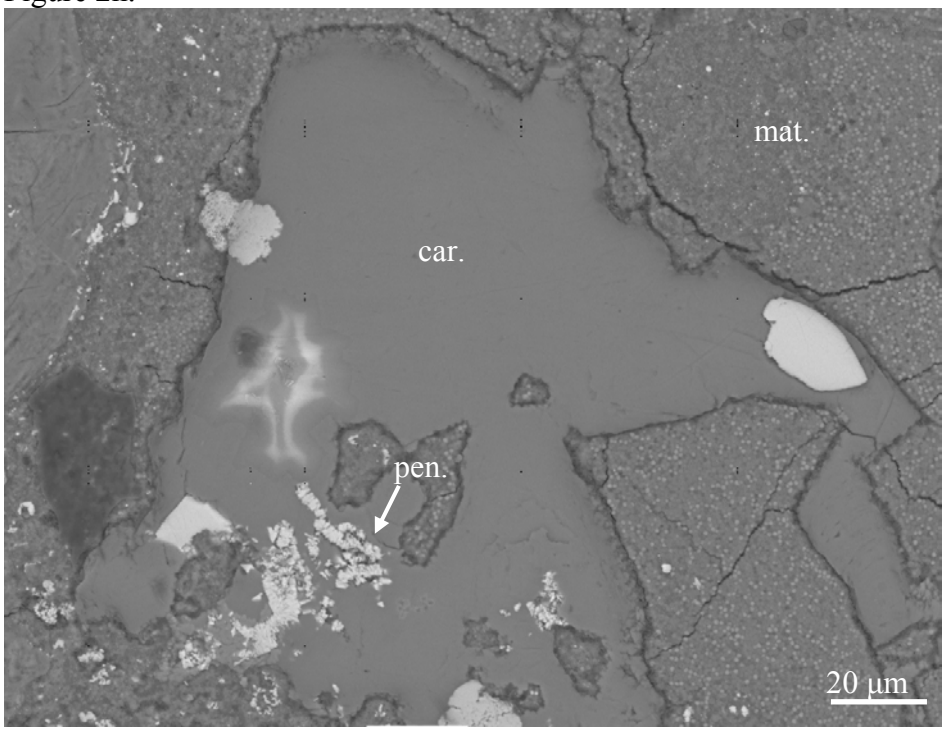

841
842 Figure 3

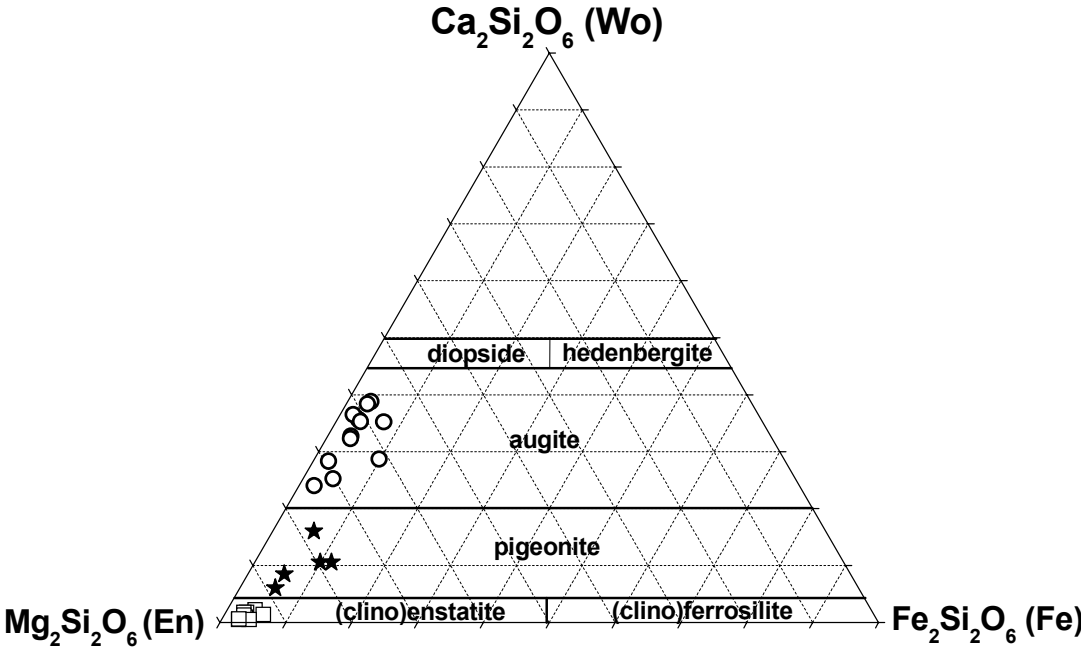

843
844
845 Figure 4

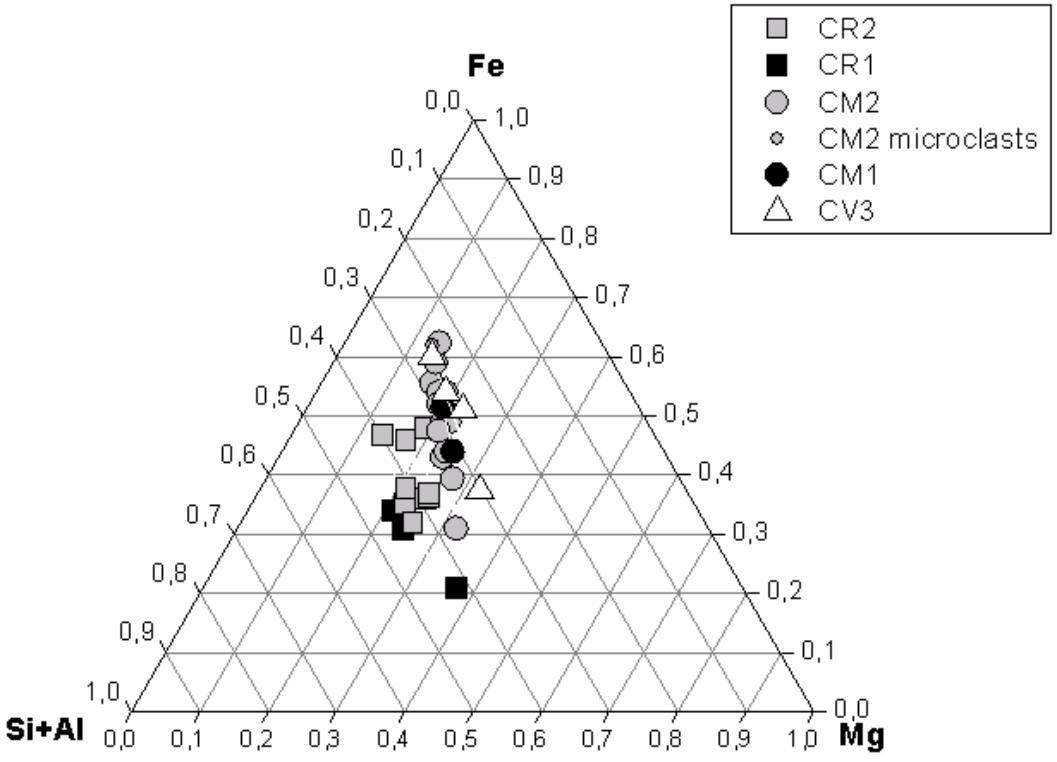

846

847

848 Figure 5

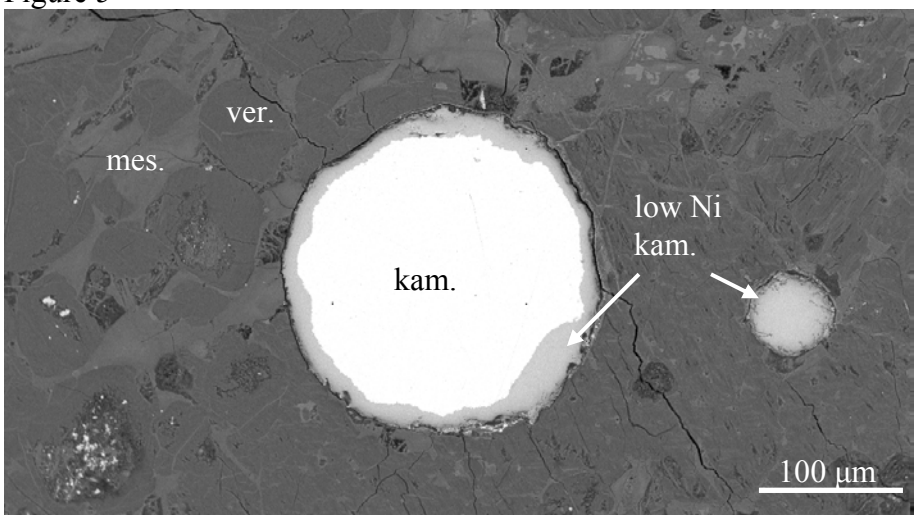

849

850 Figure 6

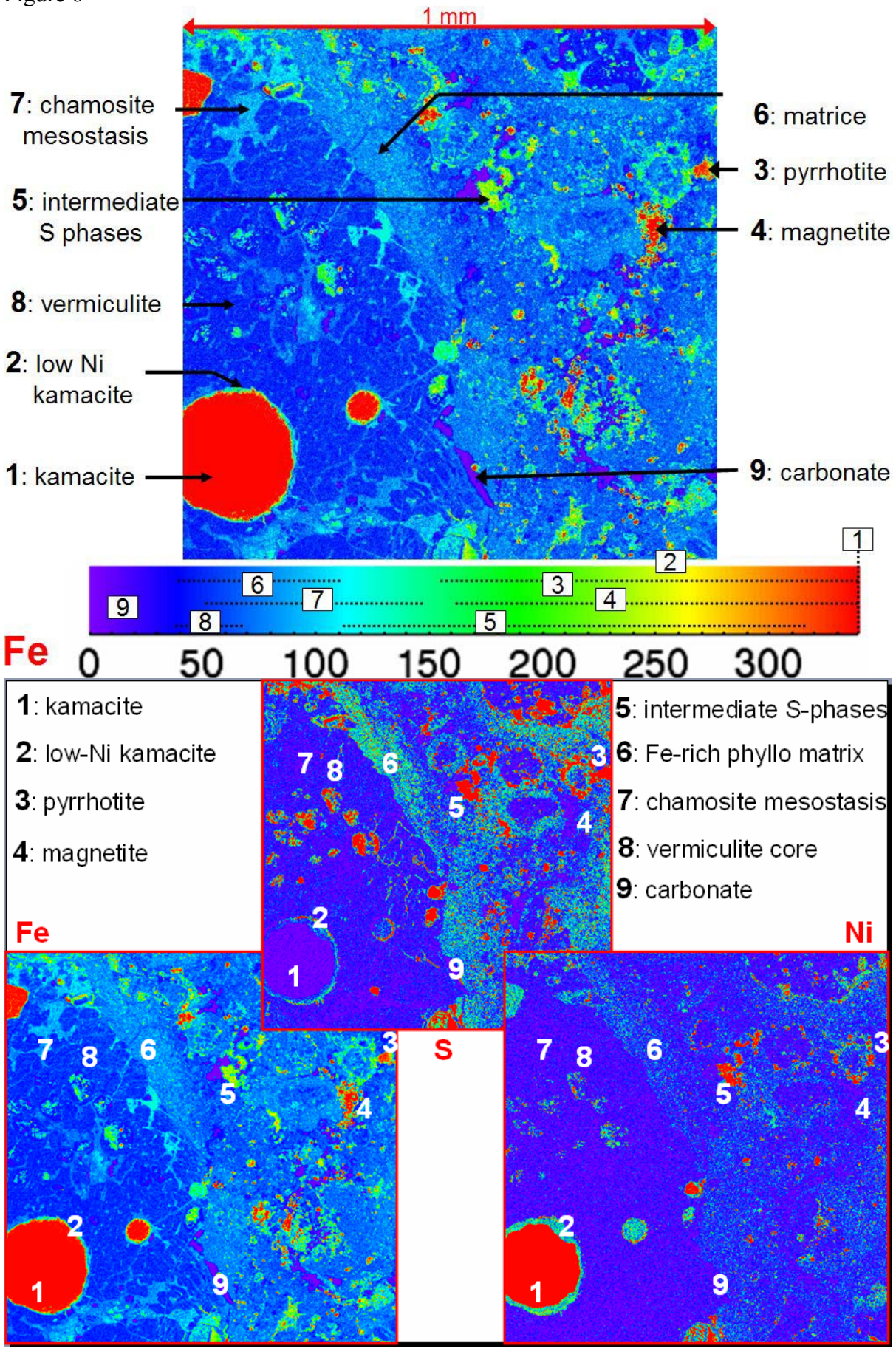

851

852

853 Figure 7

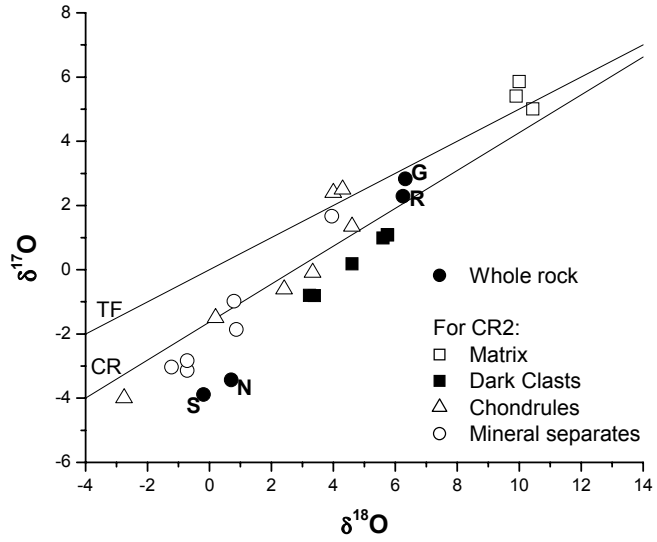

854
855 Figure 8

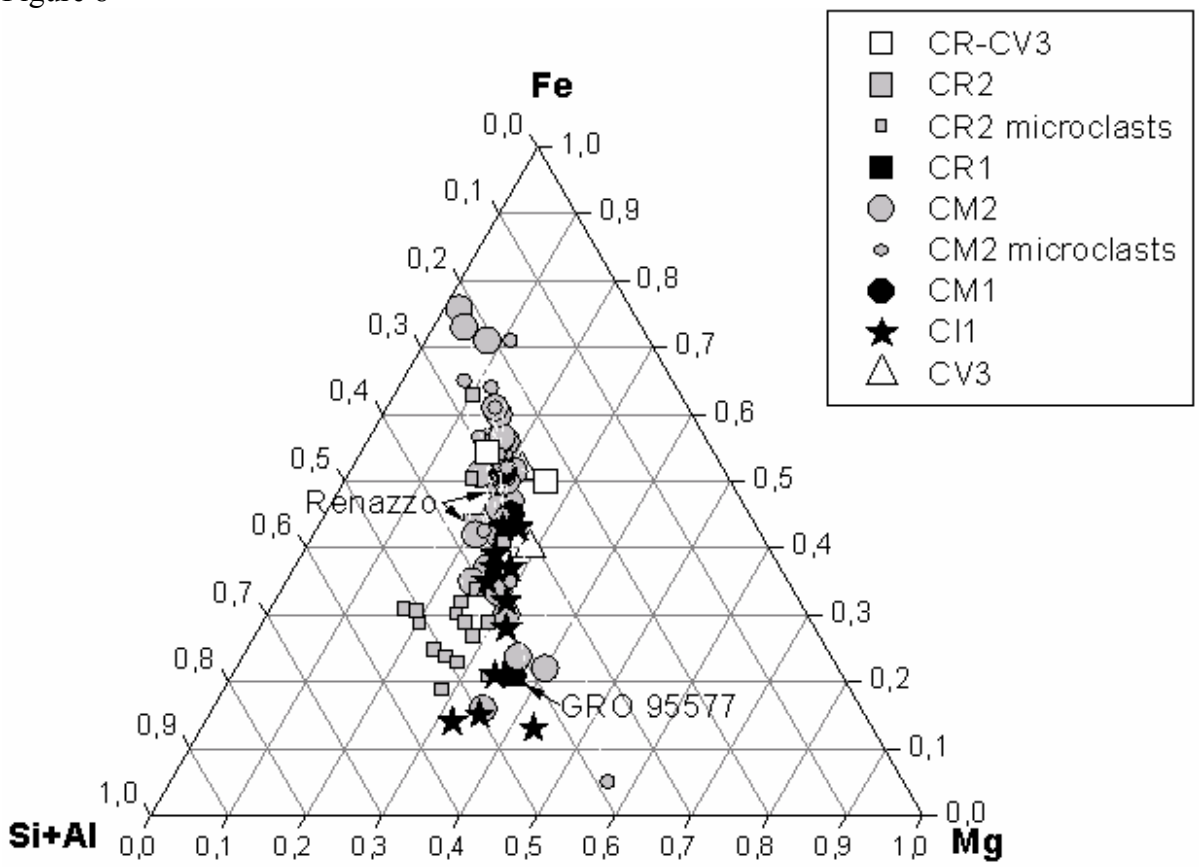

856
857

FIGURE CAPTIONS

Figure 1. BSE image of a part of Renazzo thick section.

Figure 1a. Colored X-ray elemental maps of Ca, Fe, Ni, S and octovertet ratio of the area a in Figure 1.

Figure 1b. BSE image of a porphyritic type I chondrule having olivine and pyroxene core and feldspathic mesostasis in Renazzo. kam: kamacite, low-Ni kam: low-Ni kamacite, ol: olivine, px: pyroxene, mes: mesostasis, mat: matrix, car: Ca-rich carbonate.

Figure 1c. BSE image of porphyritic type II chondrule having Fe-olivine core and chamosite mesostasis in Renazzo. int. S phases: intermediate sulfide phases, Fe-ol: Fe-rich olivine.

Figure 1d. BSE image of the contact between Fe-olivine core and chamosite mesostasis in type II chondrule of Renazzo. PP: porphyritic pyroxene chondrule, POP: porphyritic olivine pyroxene chondrule, low-Ni kam.:low-Ni kamacite, mat: matrix.

Figure 1e. BSE image of the contact between matrix and PP and POP chondrules in Renazzo.

Figure 2. BSE image of GRO 95577 thick section.

Figure 2a. BSE image of a porphyritic chondrule having vermiculite core and chamosite mesostasis in GRO 95577.

Figure 2b. BSE image of the contact between vermiculite core and chamosite mesostasis in GRO 95577 chondrule. low-Ni kam.: low-Ni kamacite, mag: magnetite, pen: pentlandite, ver.: vermiculite, mes: mesostasis, car:Ca-rich carbonate.

Figure 2c. BSE image of the contact between vermiculite core and chamosite mesostasis in an altered barred-olivine chondrule of GRO 95577. ver: vermiculite, clin. mes.: clinochlore mesostasis.

Figure 2d. BSE image of a low-Ni kamacite bleb within GRO 95577 chondrule. low-Ni kam.: low-Ni kamacite.

Figure 2e. BSE image of pyrrhotite at the border between chondrule and matrix within GRO 95577. Po: pyrrhotite, ver.: vermiculite, mat: matrix.

Figure 2f. BSE image of intermediate sulfide phases at the border between chondrule and matrix within GRO 95577. int. S phases: intermediate S phases., mat: matrix.

Figure 2g. BSE image of fine-grained matrix of GRO 95577 in which magnetite are observed. mag: magnetite, mat.:matrix.

Figure 2h. BSE image of large calcite, in which pentlandite are observed, within GRO 95577 matrix. pen.:pentlandite, mat: matrix, car: Ca-rich carbonate.

907 Figure 3. Compositions of the pyroxenes within Renazzo chondrules plotted in a Fe-Wo-En
908 ternary diagram.
909
910 Figure 4. Compositions of the phyllosilicates from Renazzo and GRO 95577 chondrules
911 plotted in a Mg-Fe-Si+Al ternary diagram and compared to phyllosilicates composition from
912 other CRS, CMs and CVs chondrules.
913
914 Figure 5. BSE image of zoned kamacite within GRO 95577 chondrule. The inner part is Ni-
915 richer than the outer part of the bleb. low-Ni kam.: low-Ni kamacite, kam: kamacite,
916 ver.:vermiculite, clin. mes.: clinochlore mesostasis.
917
918 Figure 6. X-ray elemental maps (1000 * 1000 μm^2) for Fe, Ni and S on GRO 95577. 1
919 kamacite, 2 low-Ni kamacite, 3 pyrrhotite, 4 magnetite, 5 intermedite phases, 6 Fe-rich
920 phyllosilicate matrix, 7 chamosite rich mesostasis, 8 vermiculite, 9 carbonate.
921
922 Figure 7. Oxygen three-isotope graph showing the whole rock composition of Renazzo (R)
923 (Weisberg et al. 1993) and GRO 95577 (G) (Weisberg and Prinz 2000) but also of the two
924 CR-CV3 chondrites NWA 1152 (N) and SAH 00182 (S) (both from Smith et al. 2004). The
925 composition of matrices, dark clasts, chondrules and mineral separates from CR2 are also
926 plotted (from Weisberg et al. 1993). TF=terrestrial fractionation line, CR="CR-clan" line.
927
928 Figure 8. Compositions of the phyllosilicates from Renazzo and GRO 95577 matrices plotted
929 in a Mg-Fe-Si+Al ternary diagram and compared to phyllosilicates composition from other
930 CRS, CMs, CIs and CVs matrices.